Exploiting NOMA and RIS in Integrated Sensing and Communication

Jiakuo Zuo, Yuanwei Liu, *Senior Member, IEEE*, Chenming Zhu, Yixuan Zou, *Graduate Student Member, IEEE*, Dengyin Zhang and Naofal Al-Dhahir, *Fellow, IEEE*

Abstract

A novel integrated sensing and communication (ISAC) system is proposed, where a dual-functional base station is utilized to transmit the superimposed non-orthogonal multiple access (NOMA) communication signal for serving communication users and sensing targets simultaneously. Furthermore, a new reconfigurable intelligent surface (RIS)-aided-sensing structure, where a dedicated RIS is deployed to provide virtual line-of-sight (LoS) links for radar targets, is also proposed to address the significant path loss or blockage of LoS links for the sensing task. Based on this setup, the beampattern gain at the RIS for the radar target is derived and adopted as a sensing metric. The objective of this paper is to maximize the minimum beampattern gain by jointly optimizing active beamforming at the base station (BS), power allocation coefficients among NOMA users and passive beamforming at the RIS. To tackle the non-convexity of the formulated optimization problem, the beampattern gain and constraints are first transformed into more tractable forms. Then, an iterative block coordinate descent (IBCD) algorithm is proposed by employing successive convex approximation (SCA), Schur complement, semidefinite relaxation (SDR) and sequential rank-one constraint relaxation (SRCR) methods. To reduce the complexity of the proposed IBCD algorithm, a low-complexity iterative alternating optimization (IAO) algorithm is proposed. Particularly, the active beamforming is optimized by solving a semidefinite programming (SDP) problem and the closed-form solutions of the power allocation coefficients are derived. Numerical results show that: i) the proposed RIS-NOMA-ISAC system always outperforms the RIS-ISAC system

J. Zuo is with the Institute of Communications and Information Technology, China Information Consulting and Designing Institute Company Ltd., Nanjing 210003, China, and also with School of Internet of Things, Nanjing University of Posts and Telecommunications, Nanjing, China. (email:zuojiakuo@njupt.edu.cn).

Y. Liu and Y. Zou are with the School of Electronic Engineering and Computer Science, Queen Mary University of London, London E1 4NS, U.K. (e-mail:yuanwei.liu@qmul.ac.uk, yixuan.zou@qmul.ac.uk).

C. Zhu is with the Institute of Communications and Information Technology, China Information Consulting and Designing Institute Company Ltd., Nanjing 210003, China. (email:e-mail: zhuchenming@cicdi.com).

D. Zhang is with School of Internet of Things, Nanjing University of Posts and Telecommunications, Nanjing, China. (email:zhangdy@njupt.edu.cn).

N. Al-Dhahir is with the Department of Electrical and Computer Engineering, The University of Texas at Dallas, Richardson, TX 75080 USA. (email:aldhahir@utdallas.edu).

without NOMA in beampattern gain and illumination power; ii) the low-complexity IAO algorithm achieves a comparable performance to that achieved by the IBCD algorithm. iii) high beampattern gain can be achieved by the proposed joint optimization algorithms in underloaded and overloaded communication scenarios.

Index Terms

Beamforming optimization, integrated sensing and communication, non-orthogonal multiple access, reconfigurable intelligent surface.

I. INTRODUCTION

For conventional wireless communication systems, the main performance indicator is the communication quality of service (QoS). However, in the upcoming beyond fifth generation (B5G) and sixth generation (6G) wireless networks, sensing service will play a more important role than ever before [2, 3]. The goal of future wireless communication is to provide services based on both sensing and communication functionalities. Toward this goal, integrated sensing and communication (ISAC) has emerged and attracted growing attention in both academia and industries [2, 4, 5]. Broadly, the research contributions on ISAC can be classified into two categories, namely, radar-communication coexistence (RCC) and dual-function radar communication (DFRC) [6]. For RCC, the radar and communication devices are separated, while the spectrum is shared simply by radar and communication systems. Sophisticated interference management and cooperation techniques are needed for RCC to mitigate the system interference. However, this requires a large number of information exchanges and leads to high overhead. For DFRC, the radar and communication functions share the same hardware and a unified transmit waveform is exploited to simultaneously perform communication and sensing tasks. Nevertheless, it is a challenging task to design an efficient waveform to balance the conflicting requirements between the communication and sensing tasks.

Various key techniques, such as millimeter wave (mmWave) [7–9], terahertz (THz) [10–12], massive multiple-input multiple-output (MIMO) [13] and multi-unmanned aerial vehicle (UAV) [11, 14], have been incorporated in ISAC systems to boost the communication and sensing capabilities, Given the already large number of works on ISAC communications, in this paper we focus on the applications of non-orthogonal multiple access (NOMA) and reconfigurable intelligent surface (RIS) to ISAC (or DFRC) systems.

A. Prior Works

A handful of works have been devoted to studying NOMA-ISAC and RIS-ISAC systems. We elaborate on them as follows.

1) Studies on NOMA-ISAC systems: NOMA has received significant attention as a promising technique for supporting massive connectivity, interference management, and spectrum enhancement [15, 16]. The authors of [17] first proposed a novel NOMA-aided joint radar and multicast-unicast communication system, where the base station (BS) transmits superimposed multicast and unicast messages to the radar users and communication users, while detecting the radar user targets. The authors of [18] utilized the superimposed NOMA communication signal to perform radar sensing and proposed a beamforming design algorithm to maximize the weighted sum of the communication throughput and the effective sensing power. Since the sensing signal can also be information-bearing, the authors of [19] utilized multiple beams of the sensing signal to deliver extra multicast information while detecting radar targets. The communication users received one desired unicast stream and multiple multicast streams, which were detected by successive interference cancellation (SIC). In conventional ISAC networks, the total bandwidth was assumed to be utilized for both radar detection and wireless communication. However, this assumption is impractical because the bandwidth is occupied by different applications. To overcome this difficulty, the authors of [20] proposed an uplink NOMA-assisted semi-ISAC system, where the total bandwidth was divided into three portions, namely the ISAC bandwidth, the communication-only bandwidth, and the sensing-only bandwidth.

2) Studies on RIS-ISAC systems: Although many key enablers, such as mmWave, MIMO and THz, have demonstrated tremendous potential in improving the performances of the ISAC system, they usually suffer from various practical limitations, such as uncontrollable electromagnetic waves propagation, high hardware complexity and energy consumption [6]. Recently, a novel energy-efficient technique, namely, RIS [21], has been proposed as an important enabling technology for enhancing the communication performance. By smartly adjusting the amplitude and phase response of the reflecting elements, RIS can reconfigure the electromagnetic environments. Furthermore, by deploying RIS, additional optimization degrees of freedoms (DoFs) and virtual line-of-sight (LoS) links can be introduced for radar targets. In [22], the authors considered two scenarios for RIS-ISAC systems. In the first scenario, the users and targets were well separated and a single RIS was deployed to enhance the communication performance. The transmit beam-

formers and RIS phase shifts were designed by minimizing the total beampattern mismatch error and the average squared cross-correlation. In the second scenario, two geographically separated RISs were deployed for sensing and communications. The transmit beamformers and RIS phase shifts were optimized by maximizing the worst-case target illumination power. The authors of [23] studied the transmit power minimization problem and considered two cases. For case 1, the interference introduced by the RIS was perfectly canceled and the cross correlation design was ignored. For case 2, both the interference introduced by the RIS and the cross-correlation pattern design were considered. In addition, the authors proved that the dedicated radar signals were not required in case 1, while the dedicated radar signals were required in case 2 to enhance the system performance. The authors of [24] leveraged RIS to assist a mmWave ISAC system and proposed a novel passive beamforming strategy by considering the target size. The closed-form detection probability for target sensing was derived and a new concept of ultimate detection resolution was introduced to measure the target detection capability. Furthermore, the resource allocation for mmWave ISAC system was studied in [25], where the authors formulated a sum-rate maximization problem and derived closed-form expressions for the radar signal covariance matrix, the communication beamforming vectors and the RIS phase shifts. For THz ISAC system, the authors of [26] explored the implementation of RIS to compensate for the path loss caused by molecular absorption. In addition, a joint beamforming optimization algorithm was proposed, which utilized gradient-based, primal-dual proximal policy optimization in the multi-user multiple-input single-output (MISO) scenario. In practical scenarios, the LoS link between the BS (or access point) and the sensing targets is likely to be blocked. As a result, target sensing is not applicable. To resolve this issue, the authors of [27, 28] utilized RIS to establish virtual LoS links for target sensing and proposed efficient passive beamforming optimization algorithms to guarantee the targets sensing performance. However, the prior works were focused on the traditional reflection-only RIS, which requires the users and targets to be located at the same side of the BS and RIS. To overcome this limitation, the authors of [29] proposed a simultaneously transmitting and reflecting intelligent surface (STARS) enabled ISAC system, where STARS can provide 360° full-space coverage and divide the whole space into two half-spaces, namely the communication space and the sensing space.

B. Motivations and Contributions

Motivated by the aforementioned NOMA-ISAC and RIS-ISAC systems, this paper aims to achieve further performance enhancement by investigating the integration of NOMA and RIS

in ISAC systems. The RIS-NOMA-ISAC system is still a nascent field and many open issues deserve exploration. Note that the integration of NOMA and RIS in an ISAC system will provide more DoFs for system design and optimization, which makes the optimization problem different from that of the NOMA-ISAC system or RIS-ISAC system. The motivations and challenges of this paper can be summarized as follows.

- In future ISAC networks, a massive number of devices will be connected to the networks. The communication users and radar targets will suffer from severe interference. Although multi-antenna techniques can be employed to mitigate the inter-user interference, they cannot efficiently support both communication and sensing functions due to the limited spatial DoFs, which motivates us to consider the NOMA technique. By applying SIC, NOMA can reduce the impact of limited spatial DoFs, by partially removing inter-user interference and supporting more communication users with the same orthogonal resource.

- In conventional ISAC systems, radar sensing relies on LoS links between BS and radar targets, while the direct communication links between the BS and users are generally assumed to be available. However, in practical scenarios, the radar targets are likely to be distributed in the non-LoS (NLoS) region of the BS and the direct communication links are often blocked, which motivates us to apply the RIS technique to provide virtual LoS links and reflection links for radar sensing and communication, respectively.

- By exploiting NOMA and RIS techniques, more DoFs can be introduced to enhance the design flexibility of ISAC systems. However, more optimization variables are introduced and the optimization complexity increases. Specifically, it is still a challenging issue to jointly optimize the active beamforming at the BS, the power allocation among NOMA users, and the passive beamforming at the RIS, while guaranteeing the radar-specific requirements and QoS requirements of communication users.

Inspired by the aforementioned research, motivations and challenges, this paper focus on the design of the RIS-NOMA-ISAC system. To the best of our knowledge, the joint optimization design of the considered system has not been studied yet. Our contributions are summarized as follows.

1) We propose a novel RIS-NOMA-ISAC system with a RIS-aided-sensing structure, where a dedicated RIS is leveraged to introduce virtual LoS links for target sensing and to establish reflection links for user communication. Based on this, we derive the beampattern

gain at the RIS as the sensing metric. In addition, to achieve high spectral efficiency, we exploit the SIC technique of NOMA to multiplex communication users and to mitigate the inter-user interference. To improve the sensing performance while guaranteeing the minimum QoS required for the communication users, we formulate the beampattern gain maxmin optimization problem by jointly optimizing active beamforming, power allocation coefficients, and passive beamforming.

2) The main challenges of solving the formulated problem is the high coupling between the optimization variables and the exponential expressions of RIS phase shifts. We propose an iterative block coordinate descent (IBCD) algorithm to solve the formulated optimization problem. In particular, we first transform the optimization problem into a more tractable form, then we divide the coupled variables into two blocks. Finally, we exploit semidefinite relaxation (SDR), successive convex approximation (SCA), and the sequential rank-one constraint relaxation (SRCR) algorithm to solve the resultant problems.

3) To reduce the complexity of the proposed IBCD algorithm, we further develop a low-complexity iterative alternating optimization (IAO) algorithm, where we derive closed-form solutions for the power allocation coefficients in each NOMA cluster and obtain the active beamforming solution by solving a semidefinite programming (SDP) problem.

4) Our simulation results verify the effectiveness of the proposed algorithms and demonstrate the superior ISAC performance of the proposed RIS-NOMA-ISAC system over the RIS-ISAC system without NOMA. We also obtain some insights from the simulation results. Firstly, the IBCD algorithm outperforms the IAO algorithm but has a higher complexity. Secondly, the proposed RIS-NOMA-ISAC system can achieve high sensing performance for underloaded and overloaded communication scenarios.

C. Organization

The rest of this paper is organized as follows. In Section II, the system model and the problem formulation for designing the RIS-NOMA-ISAC system are presented. In Sections III and IV, we present the proposed IBCD algorithm and IAO algorithm to solve the original optimization problem, respectively. Numerical results are presented in Section V, which is followed by the conclusions in Section VI.

Notations: $\mathbb{C}^{M \times 1}$ denotes the space of $M \times 1$ complex valued vectors, diag($\mathbf{x}$) denotes a diagonal matrix whose diagonal elements correspond to vector $\mathbf{x}$. The (m, n)-th element of
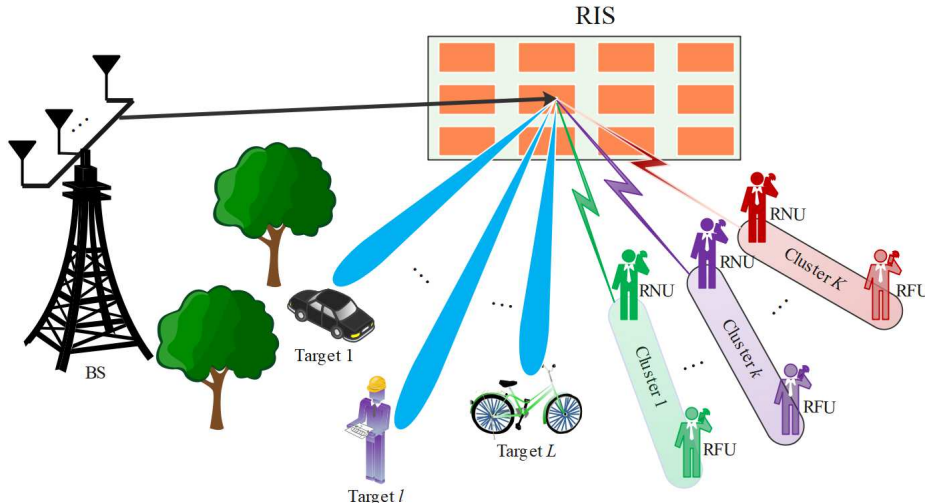
Fig. 1: Illustration of the proposed RIS-NOMA-ISAC system.

matrix $\mathbf{X}$ is denoted as $[\mathbf{X}]_{m,n}$. $\mathbf{x}^H$ and $\mathbf{X}^H$ denote the conjugate transpose of vector $\mathbf{x}$ and matrix $\mathbf{X}$, respectively. The notations $\text{Tr}(\mathbf{X})$ and $\text{rank}(\mathbf{X})$ denote the trace and rank of matrix $\mathbf{X}$, respectively. $\mathcal{CN}(0, \sigma^2)$ represents the distribution of a circularly symmetric complex Gaussian variable (CSCG) with zero mean and σ^2 variance.

II. System Model and Problem Formulation

As shown in Fig. 1, a RIS-NOMA-ISAC system is proposed, which consists of a dual-functional BS equipped with N antennas, $2K$ single-antenna users, a uniform linear array (ULA)-RIS with M reflecting elements, and L radar targets. We assume that all the direct links from the BS to the communication users and to the radar targets are blocked, which prevents the BS from performing communication and sensing tasks. By carefully deploying the RIS, virtual LoS links can be established from the BS to the communication users and to the radar targets. Thus, the performance of communication and sensing tasks can be significantly enhanced. To improve the spectral efficiency and to reduce the system load, we assume that the $2K$ users are grouped into K clusters by employing user clustering techniques[1]. As a result, there are two users in each cluster, namely the RIS-near user (RNU) and the RIS-far user (RFU). Generally, the RNUs are much closer to the RIS than the RFUs. In each cluster, the NOMA protocol is applied to serve all users with the same orthogonal resource. The cluster and user sets are denoted by $\mathcal{K} = \{1, \cdots, K\}$ and $\mathcal{U} = \{1, \cdots, 2K\}$, respectively. Moreover, $\mathcal{U}_k$ denotes the set of users

---

[1]Many efficient user clustering methods have been proposed for NOMA systems, such as: many-to-one matching [16], K-means [30], and correlation of channels [31]. These methods can also be applied for our considered system. In this paper, we only focus on the system optimization problem after user clustering.

in cluster k, where $\mathcal{U} = \cup_{k \in \mathcal{K}} \mathcal{U}_k$, $\mathcal{U}_k \cap \mathcal{U}_{\underline{k}} = \oslash (k, \underline{k} \in \mathcal{K}, k \neq \underline{k})$. For notation simplicity, we denote the RNU and RFU in the k-th cluster as users $\mathrm{U}(k, n)$ and $\mathrm{U}(k, f)$, respectively.

A. Communication Model

The superimposed communication signal transmitted by the BS is given by

$$\mathbf{x} = \sum_{k=1}^{K} \mathbf{w}_k \left(\sqrt{a_{k,n}} s_{k,n} + \sqrt{a_{k,f}} s_{k,f} \right), \tag{1}$$

where $\mathbf{w}_k \in \mathbb{C}^{N \times 1}$ is the active beamforming vector of the k-th cluster, $s_{k,i}$ denotes the communication signal to be sent to user $\mathrm{U}(k, i)$ with $\mathbb{E}\left(s_{k,i}^H s_{k,i} \right) = 1$, and $a_{k,i}$ is the corresponding power allocation coefficient, $i \in \{n, f\}$, $k \in \mathcal{K}$.

Let $\mathbf{G} \in \mathbb{C}^{M \times N}$ and $\mathbf{g}_{k,i} \in \mathbb{C}^{M \times 1}$ be the channel coefficients of the communication links $\mathrm{BS} \to \mathrm{RIS}$ and $\mathrm{RIS} \to \mathrm{U}(k, i)$, respectively. Furthermore, let $\mathbf{v} = \left[e^{j\theta_1^{\mathrm{RIS}}} e^{j\theta_2^{\mathrm{RIS}}} \cdots e^{j\theta_M^{\mathrm{RIS}}} \right]$ be the passive beamforming vector with $\theta_m^{\mathrm{RIS}} \in [0, 2\pi)$ denoting the phase shift of the m-th reflecting element, $m \in \mathcal{M} \triangleq \{1, 2, \cdots, M\}$. With the help of RIS, the signal received at user $\mathrm{U}(k, i)$ can be mathematically expressed as

$$y_{k,i} = \underbrace{\left(\mathbf{g}_{k,i}^H \boldsymbol{\Theta} \mathbf{G} \right) \mathbf{w}_k \sqrt{a_{k,i}} s_{k,i}}_{\text{desired signal}} + \underbrace{\left(\mathbf{g}_{k,i}^H \boldsymbol{\Theta} \mathbf{G} \right) \mathbf{w}_k \sqrt{a_{k,\widetilde{i}}} s_{k,\widetilde{i}}}_{\text{intra-cluster interference}} + \underbrace{\left(\mathbf{g}_{k,i}^H \boldsymbol{\Theta} \mathbf{G} \right) \sum_{\widetilde{k} \neq k}^{K} \mathbf{w}_{\widetilde{k}} \sum_{j \in \{n,f\}} \sqrt{a_{\widetilde{k},j}} s_{\widetilde{k},j}}_{\text{inter-cluster interference}} + \underbrace{z_{k,i}}_{\text{noise}}, \tag{2}$$

with $\widetilde{i}, i \in \{n, f\}$ and $\widetilde{i} \neq i$, where $\boldsymbol{\Theta} = \mathrm{diag}(\mathbf{v})$ is the RIS's diagonal phase shift matrix and $z_{k,i} \sim \mathcal{CN}(0, \sigma^2)$ is the additive white Gaussian noise (AWGN).

In the proposed RIS-NOMA-ISAC system, SIC is applied for the users to decode their signals in each cluster. We assume a fixed decoding order in each cluster. Particularly, user $\mathrm{U}(k, n)$ first decodes the signal of user $\mathrm{U}(k, f)$ and then subtracts it from its observation to decode its own information. Therefore, the achievable rate for user $\mathrm{U}(k, n)$ to decode the signal of user $\mathrm{U}(k, f)$ is given by

$$R_{k, f \to n} = \log_2 \left(1 + \frac{a_{k,f} \left| \mathbf{g}_{k,n}^H \boldsymbol{\Theta} \mathbf{G} \mathbf{w}_k \right|^2}{I_{k,n}^{\mathrm{itra}} + I_{k,n}^{\mathrm{iter}} + \sigma^2} \right), \tag{3}$$

where $I_{k,n}^{\mathrm{itra}} = a_{k,n} \left| \mathbf{g}_{k,n}^H \boldsymbol{\Theta} \mathbf{G} \mathbf{w}_k \right|^2$ and $I_{k,n}^{\mathrm{iter}} = \sum_{\widetilde{k} \neq k}^{K} \left| \mathbf{g}_{k,n}^H \boldsymbol{\Theta} \mathbf{G} \mathbf{w}_{\widetilde{k}} \right|^2$.

If the above decoding is successful, user $\mathrm{U}(k, n)$ removes the signal $s_{k,f}$ from $y_{k,n}$ to further decode its own signal $s_{k,n}$. Therefore, the individual achievable rate of user $\mathrm{U}(k, n)$ is given by

$$R_{k,n} = \log_2 \left(1 + \frac{a_{k,n} \left| \mathbf{g}_{k,n}^H \boldsymbol{\Theta} \mathbf{G} \mathbf{w}_k \right|^2}{I_{k,n}^{\mathrm{iter}} + \sigma^2} \right). \tag{4}$$

Accordingly, user $\mathrm{U}(k, f)$ directly decodes its own signal by treating the other users' signals as interference. Therefore, the achievable rate for user $\mathrm{U}(k, f)$ to decode its own signal can be expressed as

$$R_{k,f \to f} = \log_2 \left(1 + \frac{a_{k,f} \left| \mathbf{g}_{k,f}^H \boldsymbol{\Theta} \mathbf{G} \mathbf{w}_k \right|^2}{I_{k,f}^{\mathrm{itra}} + I_{k,f}^{\mathrm{iter}} + \sigma^2} \right), \tag{5}$$

where $I_{k,f}^{\mathrm{itra}} = a_{k,n} \left| \mathbf{g}_{k,f}^H \boldsymbol{\Theta} \mathbf{G} \mathbf{w}_k \right|^2$ and $I_{k,f}^{\mathrm{iter}} = \sum_{\tilde{k} \neq k}^{K} \left| \mathbf{g}_{k,f}^H \boldsymbol{\Theta} \mathbf{G} \mathbf{w}_{\tilde{k}} \right|^2$.

As a result, the individual achievable rate of user $\mathrm{U}(k, f)$ is given by [32, 33]

$$R_{k,f} = \min \left\{ R_{k,f \to n}, R_{k,f \to f} \right\}. \tag{6}$$

B. Radar Detection Model

Since all the potential targets are in the NLoS areas of the BS, no LoS links from the BS can be exploited to perform radar target sensing. However, we can utilize the reflection-LoS links created by the RIS to complete the sensing tasks. We consider using the RIS's beampattern gain as the sensing performance metric. The reflected signal at the RIS can be expressed as

$$\overline{\mathbf{x}} = \boldsymbol{\Theta} \mathbf{G} \left(\sum_{k=1}^{K} \mathbf{w}_k \left(\sqrt{a_{k,n}} s_{k,n} + \sqrt{a_{k,f}} s_{k,f} \right) \right). \tag{7}$$

Therefore, the corresponding covariance matrix is given by

$$\mathbf{R}_{\overline{\mathbf{x}}} = \mathbb{E} \left(\overline{\mathbf{x}} \overline{\mathbf{x}}^H \right) = \boldsymbol{\Theta} \mathbf{G} \left(\sum_{k=1}^{K} \mathbf{w}_k \mathbf{w}_k^H \right) \mathbf{G}^H \boldsymbol{\Theta}^H. \tag{8}$$

In our considered system, the communication signal is used to perform radar target sensing, thus the RIS's beampattern gain [27] with respect to the q-th angle of interest, i.e, θ_q^{Tg}, is given by

$$\mathcal{P}_{\theta_q^{\mathrm{Tg}}} (\mathbf{w}_k, \mathbf{v}) = \boldsymbol{a}^H \left(\theta_q^{\mathrm{Tg}} \right) \boldsymbol{\Theta} \mathbf{G} \left(\sum_{k=1}^{K} \mathbf{w}_k \mathbf{w}_k^H \right) \mathbf{G}^H \boldsymbol{\Theta}^H \boldsymbol{a} \left(\theta_q^{\mathrm{Tg}} \right), \tag{9}$$

where $\boldsymbol{a}(\theta) = \left[1, e^{j \frac{2\pi d}{\lambda} \sin(\theta)}, \cdots, e^{j \frac{2\pi d}{\lambda} (M-1) \sin(\theta)} \right]^T$ is the steering vector at the RIS with angle θ, d denotes the antenna spacing, λ denotes the carrier wavelength, $q \in \mathcal{Q} \triangleq \{1, 2, \cdots, Q\}$, and $\mathcal{Q}_\theta = \left\{ \theta_1^{\mathrm{Tg}}, \theta_2^{\mathrm{Tg}}, \cdots, \theta_Q^{\mathrm{Tg}} \right\}$ is the set of sensing angles of interest.

C. Maximize the Minimum Beampattern Gain

The objective of this paper is to maximize the minimum beampattern gain towards Q angles of interest by jointly optimizing the active beamforming, power allocation coefficients and passive

beamforming. Accordingly, the optimization problem is formulated as

$$\max_{\mathbf{a}_k, \mathbf{w}_k, \mathbf{v}} \min_{q \in \mathcal{Q}} \mathcal{P}_{\theta_q^{\mathrm{Tg}}} (\mathbf{w}_k, \mathbf{v}), \tag{10a}$$

$$\text{s.t. } R_{k,i} \geqslant R_{k,i}^{\min}, \tag{10b}$$

$$\sum_{k=1}^{K} \|\mathbf{w}_k\|_2 \leqslant P_{\max}, \tag{10c}$$

$$a_{k,n} + a_{k,f} = 1, a_{k,i} \in (0,1), \tag{10d}$$

$$\theta_m^{\mathrm{RIS}} \in [0, 2\pi), \tag{10e}$$

where $R_{k,i}^{\min}$ is the minimum QoS requirement, $P_{\max}$ is the maximum transmit power at the BS, $\mathbf{a}_k = [a_{k,n} \ a_{k,f}]^T$, $i \in \{n, f\}$, $k \in \mathcal{K}$, $m \in \mathcal{M}$. Constraint (10b) ensures the minimum QoS requirement of each NOMA user, constraint (10c) limits the maximum transmit power at the BS, constraint (10d) represents the power allocation coefficient constraint in each cluster, and constraint (10e) is the phase shift constraint for the RIS.

Due to the coupling between $\mathbf{w}_k$, $\mathbf{a}_k$ and $\mathbf{v}$, the non-convexity of QoS constraints, and the exponential form of phase shifts in $\mathbf{v}$, problem (10) is a highly nonconvex optimization problem and the optimal solution is in general intractable. In the next section, a suboptimal IBCD algorithm is proposed to solve problem (10).

III. Proposed Solution

In this section, we elaborate on how to solve problem (10). We first transform problem (10) into a more tractable form. To facilitate the design, we define $\mathbf{W}_k = \mathbf{w}_k \mathbf{w}_k^H$, where $\mathbf{W}_k$ satisfies $\mathbf{W}_k \succeq \mathbf{0}$ and $\mathrm{rank}\,(\mathbf{W}_k) = 1$, $k \in \mathcal{K}$. Similarly, we define $\mathbf{V} = \mathbf{v}^H \mathbf{v}$, which needs to satisfy $\mathbf{V} \succeq \mathbf{0}$ and $\mathrm{rank}\,(\mathbf{V}) = 1$. Then, the beampattern gain in (9) can be rewritten as:

$$\mathcal{P}_{\theta_q^{\mathrm{Tg}}} (\mathbf{W}_k, \mathbf{V}) = \mathrm{Tr}\left[\mathbf{V} \mathbf{\Upsilon}_q \left(\sum_{k=1}^{K} \mathbf{W}_k \right) \mathbf{\Upsilon}_q^H \right], \tag{11}$$

where $\mathbf{\Upsilon}_q = \mathrm{diag}\left\{ \boldsymbol{a}^H \left(\theta_q^{\mathrm{Tg}} \right) \right\} \mathbf{G}$.

Moreover, the quadratic terms $\left| \mathbf{g}_{k,i}^H \mathbf{\Theta} \mathbf{G} \mathbf{w}_k \right|^2$ and $\left| \mathbf{g}_{k,i}^H \mathbf{\Theta} \mathbf{G} \mathbf{w}_{\widetilde{k}} \right|^2$ in (3), (4) and (5) can be respectively rewritten as:

$$\begin{cases} \left| \mathbf{g}_{k,i}^H \mathbf{\Theta} \mathbf{G} \mathbf{w}_k \right|^2 = \mathrm{Tr}\left(\mathbf{V} \mathbf{\Gamma}_{k,i} \mathbf{W}_k \mathbf{\Gamma}_{k,i}^H \right), \\ \left| \mathbf{g}_{k,i}^H \mathbf{\Theta} \mathbf{G} \mathbf{w}_{\widetilde{k}} \right|^2 = \mathrm{Tr}\left(\mathbf{V} \mathbf{\Gamma}_{k,i} \mathbf{W}_{\widetilde{k}} \mathbf{\Gamma}_{k,i}^H \right), k \neq \widetilde{k}, \end{cases} \tag{12}$$

where $\mathbf{\Gamma}_{k,i} = \mathrm{diag}\left\{ \mathbf{g}_{k,i}^H \right\} \mathbf{G}$, $i \in \{n, f\}$, and $k, \widetilde{k} \in \mathcal{K}$.

By exploiting the above definitions, constraints in (10b) can be equivalently reformulated as:

$$a_{k,n}\text{Tr}\left(\mathbf{V}\boldsymbol{\Gamma}_{k,n}\mathbf{W}_k\boldsymbol{\Gamma}_{k,n}^H\right) \geqslant r_{k,n}^{\min}\left(I_{k,n}^{\text{iter}} + \sigma^2\right), \tag{13}$$

$$a_{k,f}\text{Tr}\left(\mathbf{V}\boldsymbol{\Gamma}_{k,n}\mathbf{W}_k\boldsymbol{\Gamma}_{k,n}^H\right) \geqslant r_{k,f}^{\min}\left(I_{k,n}^{\text{itra}} + I_{k,n}^{\text{iter}} + \sigma^2\right), \tag{14}$$

$$a_{k,f}\text{Tr}\left(\mathbf{V}\boldsymbol{\Gamma}_{k,f}\mathbf{W}_k\boldsymbol{\Gamma}_{k,f}^H\right) \geqslant r_{k,f}^{\min}\left(I_{k,f}^{\text{itra}} + I_{k,f}^{\text{iter}} + \sigma^2\right), \tag{15}$$

where $I_{k,n}^{\text{itra}} = a_{k,n}\text{Tr}\left(\mathbf{V}\boldsymbol{\Gamma}_{k,n}\mathbf{W}_k\boldsymbol{\Gamma}_{k,n}^H\right)$, $I_{k,f}^{\text{itra}} = a_{k,n}\text{Tr}\left(\mathbf{V}\boldsymbol{\Gamma}_{k,f}\mathbf{W}_k\boldsymbol{\Gamma}_{k,f}^H\right)$, $I_{k,i}^{\text{iter}} = \sum_{\tilde{k}\neq k}^{K}\text{Tr}\left(\mathbf{V}\boldsymbol{\Gamma}_{k,i}\mathbf{W}_{\tilde{k}}\boldsymbol{\Gamma}_{k,i}^H\right)$, $r_{k,i}^{\min} = 2^{R_{k,i}^{\min}} - 1$.

Finally, the original problem (10) can be equivalently recast as follows:

$$\max_{\mathbf{a}_k,\mathbf{W}_k\succcurlyeq 0,\mathbf{V}\succcurlyeq 0}\min_{q\in\mathcal{Q}}\mathcal{P}_{\theta_q^{\text{Tg}}}\left(\mathbf{W}_k,\mathbf{V}\right), \tag{16a}$$

$$\text{s.t. } \sum_{k=1}^{K}\text{Tr}\left(\mathbf{W}_k\right) \leqslant P_{\max}, \tag{16b}$$

$$[\mathbf{V}]_{m,m} = 1, m \in \mathcal{M}, \tag{16c}$$

$$\text{rank}\left(\mathbf{W}_k\right) = 1, k \in \mathcal{K}, \tag{16d}$$

$$\text{rank}\left(\mathbf{V}\right) = 1, \tag{16e}$$

$$(10\text{d}), (13), (14), (15). \tag{16f}$$

It is noted that the objective function of problem (16) is non-smooth, hence, we introduce an auxiliary variable χ to transform the original nonsmooth optimization problem (16) into a smooth optimization problem, which is given by

$$\max_{\mathbf{a}_k,\chi>0,\mathbf{W}_k\succcurlyeq 0,\mathbf{V}\succcurlyeq 0}\chi, \tag{17a}$$

$$\text{s.t. Tr}\left[\mathbf{V}\boldsymbol{\Upsilon}_q\left(\sum_{k=1}^{K}\mathbf{W}_k\right)\boldsymbol{\Upsilon}_q^H\right] \geqslant \chi, q \in \mathcal{Q}, \tag{17b}$$

$$(10\text{d}), (13), (14), (15), (16\text{b}), (16\text{c}), (16\text{d}), (16\text{e}). \tag{17c}$$

In the remainder of this article, we utilize the IBCD approach to solve the equivalent problem (17) instead of the original problem (10). To be specific, the coupled variables are divided into two blocks, namely $\{\mathbf{W}_k, \mathbf{a}_k\}$ and $\mathbf{V}$. The active beamforming matrices $\{\mathbf{W}_k\}$ and power allocation coefficients $\{\mathbf{a}_k\}$ are first jointly optimized by applying the SCA and SDR methods. Then, the passive beamforming matrix $\mathbf{V}$ is solved by employing the SRCR algorithm [34].

A. Joint Active Beamforming and Power Allocation Coefficients Optimization

For a given passive beamforming matrix $\mathbf{V}$, the joint optimization problem for the design of $\{\mathbf{W}_k\}$ and $\{\mathbf{a}_k\}$ is given by

$$\max_{\mathbf{a}_k, \chi > 0, \mathbf{W}_k \succeq 0} \chi, \tag{18a}$$

$$\text{s.t. (10d), (13), (14), (15), (16b), (16d), (17b).} \tag{18b}$$

We note that the objective function of problem (18) is an affine function. However, $\mathbf{W}_k$ and $\mathbf{a}_k$ are coupled together in constraints (13), (14), and (15). Furthermore, the rank-one constraint (16d) is also nonconvex. As a result, these obstacles make problem (18) difficult to be solved. In the following, we will further transform and approximate problem (18) to achieve a tractable formulation.

To begin with, we define $\mathbf{H}_{k,i} = \mathbf{\Gamma}_{k,i}^H \mathbf{V} \mathbf{\Gamma}_{k,i}$, $i \in \{n, f\}$. In addition, according to the equality constraint (10d), we have: $a_{k,f} = 1 - a_{k,n}$. Then, substituting $\mathbf{H}_{k,i}$ and $a_{k,f}$ into (13), (14) and (15), we have the following equivalent inequality constraints,

$$a_{k,n} \text{Tr} \left(\mathbf{W}_k \mathbf{H}_{k,n} \right) \geqslant r_{k,n}^{\min} \left(I_{k,n}^{\text{iter}} + \sigma^2 \right), \tag{19}$$

$$\frac{r_{k,f}^{\min} \left(\frac{\text{Tr} \left(\mathbf{W}_k \mathbf{H}_{k,n} \right)}{r_{k,f}^{\min}} - I_{k,n}^{\text{iter}} - \sigma^2 \right)}{r_{k,f}^{\min} + 1} \geqslant a_{k,n} \text{Tr} \left(\mathbf{W}_k \mathbf{H}_{k,n} \right), \tag{20}$$

$$\frac{r_{k,f}^{\min} \left(\frac{\text{Tr} \left(\mathbf{W}_k \mathbf{H}_{k,f} \right)}{r_{k,f}^{\min}} - I_{k,f}^{\text{iter}} - \sigma^2 \right)}{r_{k,f}^{\min} + 1} \geqslant a_{k,n} \text{Tr} \left(\mathbf{W}_k \mathbf{H}_{k,f} \right), \tag{21}$$

where $I_{k,i}^{\text{iter}} = \sum_{\widetilde{k} \neq k}^{K} \text{Tr} \left(\mathbf{W}_{\widetilde{k}} \mathbf{H}_{k,i} \right)$.

It is observed that the functions in the left hand side of (19), and in the right hand sides of (20) and (20) have similar structure. In fact, the functions $a_{k,n} \text{Tr} \left(\mathbf{W}_k \mathbf{H}_{k,n} \right)$ and $a_{k,n} \text{Tr} \left(\mathbf{W}_k \mathbf{H}_{k,f} \right)$ are bilinear functions over $a_{k,n}$ and $\mathbf{W}_k$, which are neither convex nor concave. To develop an efficient algorithm for jointly optimizing $\{\mathbf{W}_k\}$ and $\{\mathbf{a}_k\}$, the SCA and SDR approaches are leveraged to tackle the nonconvex constraints (19), (20), and (21). In particular, we first reformulate constraint (19) by introducing a new slack variable η_k, such that

$$\begin{cases} a_{k,n} \text{Tr} \left(\mathbf{W}_k \mathbf{H}_{k,n} \right) \geqslant \eta_k^2, & (22) \\ \eta_k^2 \geqslant r_{k,n}^{\min} \left(I_{k,n}^{\text{iter}} + \sigma^2 \right). & (23) \end{cases}$$

Then, by applying the Schur complement theory [35], (22) can be further expressed in the

linear matrix inequality form, which is given by

$$\begin{bmatrix} a_{k,n} & \eta_k \\ \eta_k & \mathrm{Tr}\left(\mathbf{W}_k\mathbf{H}_{k,n}\right) \end{bmatrix} \succcurlyeq \mathbf{0}, \exists \eta_k > 0. \tag{24}$$

Furthermore, by using the SCA approach based on first-order Taylor approximation, (23) can be approximated as follows

$$\widetilde{\eta}_k^2 + 2\widetilde{\eta}_k\left(\eta_k - \widetilde{\eta}_k\right) \geqslant r_{k,n}^{\min}\left(I_{k,n}^{\mathrm{iter}} + \sigma^2\right), \tag{25}$$

where $\widetilde{\eta}_k$ is a fixed point and can be updated by $\widetilde{\eta}_k^{(t_1)} = \eta_k^{(t_1)}$, where t_1 is the iteration index.

Next, we tackle the non-convexity in constraints (20) and (21). To tackle this challenge, we resort to the arithmetic-geometric mean inequality [36]. Specifically, $a_{k,n}\mathrm{Tr}\left(\mathbf{W}_k\mathbf{H}_{k,n}\right)$ and $a_{k,n}\mathrm{Tr}\left(\mathbf{W}_k\mathbf{H}_{k,f}\right)$ can be, respectively, approximated as

$$a_{k,n}\mathrm{Tr}\left(\mathbf{W}_k\mathbf{H}_{k,n}\right) \leqslant \frac{\beta_{k,1}a_{k,n}^2}{2} + \frac{\left(\mathrm{Tr}\left(\mathbf{W}_k\mathbf{H}_{k,n}\right)\right)^2}{2\beta_{k,1}} \triangleq \mathcal{T}_{k,1}, \tag{26}$$

$$a_{k,n}\mathrm{Tr}\left(\mathbf{W}_k\mathbf{H}_{k,f}\right) \leqslant \frac{\beta_{k,2}a_{k,n}^2}{2} + \frac{\left(\mathrm{Tr}\left(\mathbf{W}_k\mathbf{H}_{k,f}\right)\right)^2}{2\beta_{k,2}} \triangleq \mathcal{T}_{k,2}, \tag{27}$$

where $\beta_{k,1}$ and $\beta_{k,2}$ are fixed points. The equality in (26) and (27) will always hold if $\beta_{k,1} = \frac{\mathrm{Tr}\left(\mathbf{W}_k\mathbf{H}_{k,n}\right)}{a_{k,n}}$ and $\beta_{k,2} = \frac{\mathrm{Tr}\left(\mathbf{W}_k\mathbf{H}_{k,f}\right)}{a_{k,n}}$.

Based on the aforementioned transformations and approximations, the constraints given in (20) and (21) can be, respectively, reformulated as

$$\frac{r_{k,f}^{\min}\left(\frac{\mathrm{Tr}\left(\mathbf{W}_k\mathbf{H}_{k,n}\right)}{r_{k,f}^{\min}} - I_{k,n}^{\mathrm{iter}} - \sigma^2\right)}{r_{k,f}^{\min} + 1} \geqslant \mathcal{T}_{k,1}, \tag{28}$$

$$\frac{r_{k,f}^{\min}\left(\frac{\mathrm{Tr}\left(\mathbf{W}_k\mathbf{H}_{k,f}\right)}{r_{k,f}^{\min}} - I_{k,f}^{\mathrm{iter}} - \sigma^2\right)}{r_{k,f}^{\min} + 1} \geqslant \mathcal{T}_{k,2}. \tag{29}$$

Finally, let us turn our attention to the rank-one constraint (16d). To address this issue, we exploit the SDR technique by removing the rank-one constraints from the problem formulation. In particular, the relaxed problem is given as

$$\max_{\chi,\eta_k>0,0<a_{k,n}<1,\mathbf{W}_k\succcurlyeq 0}\chi, \tag{30a}$$

$$\text{s.t. } (16b), (17b), (24), (25), (28), (29). \tag{30b}$$

Obviously, problem (30) is a convex SDP problem and can be efficiently solved by the CVX tool [37]. In the following theorem, we will verify the tightness of the relaxed problem (30).

Theorem 1. *If the relaxed problem* (30) *is feasible, then the solutions* $\{\mathbf{W}_k\}$ *obtained by solving problem* (30) *always satisfy* $\text{rank}(\mathbf{W}_k) \leqslant 1$, $k \in \mathcal{K}$.

Proof: Please refer to Appendix A.

Theorem 1 represents the fact that we can obtain the rank-one solutions of problem (18) by solving the convex problem (30).

Algorithm 1 Proposed joint active beamforming and power allocation coefficients optimization algorithm

---

1: **Initialize** $\beta_{k,1}^{(0)}, \beta_{k,2}^{(0)}, \widetilde{\eta}_k^{(0)}, k \in \mathcal{K}$, and set $t_1 = 0$.
2: **repeat**
3:    $t_1 = t_1 + 1$;
4:    update $\mathbf{W}_k^{(t_1)}$, $a_{k,n}^{(t_1)}$ and $\eta_k^{(t_1)}$ by solving problem (30) with given $\beta_{k,1}^{(t_1-1)}, \beta_{k,2}^{(t_1-1)}, \widetilde{\eta}_k^{(t_1-1)}$;
5:    update $\widetilde{\eta}_k^{(t_1)} = \eta_k^{(t_1)}$, $\beta_{k,1}^{(t_1)} = \frac{\text{Tr}\left(\mathbf{W}_k^{(t_1)}\mathbf{H}_{k,n}\right)}{a_{k,n}^{(t_1)}}$ and $\beta_{k,2}^{(t_1)} = \frac{\text{Tr}\left(\mathbf{W}_k^{(t_1)}\mathbf{H}_{k,f}\right)}{a_{k,n}^{(t_1)}}$;
6: **until** the objective value of problem (30) converge.
7: **Output**: $\mathbf{W}_k$ and $\mathbf{a}_k$, $k \in \mathcal{K}$.

Based on the above discussion, the proposed algorithm to solve problem (18) is summarized in **Algorithm 1**. It is noted that we need to initialize the fixed points $\left\{\beta_{k,1}^{(0)}, \beta_{k,2}^{(0)}, \widetilde{\eta}_k^{(0)}\right\}$ in **Algorithm 1**. However, it is difficult to find these feasible fixed points. In the following, we proceed to construct a feasibility problem and develop a novel feasible initial points finding algorithm. By introducing an infeasibility indicator $\delta \geq 0$, the formulated feasibility problem is given as:

$$\min_{\delta \geqslant 0, \chi > 0, 0 < a_{k,n} < 1, \mathbf{W}_k \succcurlyeq \mathbf{0}} \delta, \tag{31a}$$

$$\text{s.t. } \text{Tr}\left[\mathbf{V}\mathbf{\Upsilon}_q\left(\sum_{k=1}^{K}\mathbf{W}_k\right)\mathbf{\Upsilon}_q^H\right] + \delta \geqslant \chi, \tag{31b}$$

$$\widetilde{\eta}_k^2 + 2\widetilde{\eta}_k(\eta_k - \widetilde{\eta}_k) + \delta \geqslant r_{k,n}^{\min}\left(I_{k,n}^{\text{iter}} + \sigma^2\right), \tag{31c}$$

$$\frac{r_{k,f}^{\min}\left(\frac{\text{Tr}\left(\mathbf{W}_k\mathbf{H}_{k,n}\right)}{r_{k,f}^{\min}} - I_{k,n}^{\text{iter}} - \sigma^2\right)}{r_{k,f}^{\min} + 1} + \delta \geqslant \mathcal{T}_{k,1}, \tag{31d}$$

$$\frac{r_{k,f}^{\min}\left(\frac{\text{Tr}\left(\mathbf{W}_k\mathbf{H}_{k,f}\right)}{r_{k,f}^{\min}} - I_{k,f}^{\text{iter}} - \sigma^2\right)}{r_{k,f}^{\min} + 1} + \delta \geqslant \mathcal{T}_{k,2}, \tag{31e}$$

$$P_{\max} + \delta \geqslant \sum_{K=1}^{K}\text{Tr}(\mathbf{W}_k), \tag{31f}$$

$$(24), \tag{31g}$$

where δ denotes how far the corresponding constraint in problem (30) is from being satisfied, $q \in \mathcal{Q}$ and $k \in \mathcal{K}$.

Problem (31) is also a convex optimization problem, which can be solved efficiently. The proposed feasible points finding algorithm is summarized in **Algorithm 2**.

Algorithm 2 Feasible initial points finding algorithm

1: Randomly initialize fixed points $\beta_{k,1}^{(0)}, \beta_{k,2}^{(0)}, \widetilde{\eta}_k^{(0)}, k \in \mathcal{K}$. Let iteration index $t_2 = 0$.

2: **repeat**

3:     $t_2 = t_2 + 1$;

4:     update $\mathbf{W}_k^{(t_2)}$, $\mathbf{R}_0^{(t_2)}$ and $\eta_k^{(t_2)}$ by solving problem (31) with given $\beta_{k,1}^{(t_2-1)}, \beta_{k,2}^{(t_2-1)}, \widetilde{\eta}_k^{(t_2-1)}, k \in \mathcal{K}$;

5:     update $\widetilde{\eta}_k^{(t_2)} = \eta_k^{(t_2)}$, $\beta_{k,2}^{(t_2)} = \frac{\mathrm{Tr}\left(\mathbf{W}_k^{(t_2)}\mathbf{H}_{k,n}\right)}{a_{k,n}^{(t_2)}}$ and $\beta_{k,2}^{(t_2)} = \frac{\mathrm{Tr}\left(\mathbf{W}_k^{(t_2)}\mathbf{H}_{k,f}\right)}{a_{k,n}^{(t_2)}}$;

6: **until** δ below a predefined threshold.

7: **Output**: $\beta_{k,1}, \beta_{k,2}, \widetilde{\eta}_k, k \in \mathcal{K}$.

Remark 1. *When $\delta \to 0$, the obtained solutions of problem (31) are feasible for problem (30). Therefore, the output of **Algorithm 2** can be used to replace the initial fixed points in **Algorithm 1**.*

B. Passive Beamforming Optimization

For any given $\{\mathbf{W}_k\}$ and $\{\mathbf{a}_k\}$, the passive beamforming optimization problem is given by

$$\max_{\chi > 0, \mathbf{V} \succeq \mathbf{0}} \chi, \tag{32a}$$

$$\text{s.t. (13), (14), (15), (16c), (16e), (17b).} \tag{32b}$$

Now, the remaining non-convexity in problem (32) lies in the rank-one constraint (16e). According to the SRCR algorithm [34], the constraint $\mathrm{rank}\,(\mathbf{V}) = 1$ can be transformed equivalently as:

$$\mathbf{e}_{\max}^H\left(\mathbf{V}^{(t_3)}\right)\mathbf{V}\mathbf{e}_{\max}\left(\mathbf{V}^{(t_3)}\right) \geqslant \varepsilon^{(t_3)}\mathrm{Tr}\,(\mathbf{V}), \tag{33}$$

where $\mathbf{V}^{(t_3)}$ is the obtained solution in the t_3-th iteration, $\mathbf{e}_{\max}\left(\mathbf{V}^{(t_3)}\right)$ is the eigenvector corresponding to the maximum eigenvalue of $\mathbf{V}^{(t_3)}$, $\varepsilon^{(t_3)} \in [0, 1]$ is a relaxation parameter in the t_3-th iteration. We can increase $\varepsilon^{(t_3)}$ from 0 to 1 sequentially via iterations to gradually approach a rank-one solution. After each iteration, the relaxation parameter can be updated as

$$\varepsilon^{(t_3+1)} \longleftarrow \min\left(1, \frac{\lambda_{\max}\left(\mathbf{V}^{(t_3+1)}\right)}{\mathrm{Tr}\left(\mathbf{V}^{(t_3+1)}\right)} + \rho^{(t_3+1)}\right), \tag{34}$$

where $\lambda_{\max}\left(\mathbf{V}^{(t_3)}\right)$ is the largest eigenvalue of $\mathbf{V}^{(t_3)}$ and $\rho^{(t_3)}$ denotes the step size.

Finally, in the t_3-th iteration, the optimization problem that needs to be solved is given as follows

$$\max_{\chi > 0, \mathbf{V} \succeq \mathbf{0}} \chi, \tag{35a}$$

$$\text{s.t. } (13), (14), (15), (16c), (17b), (33). \tag{35b}$$

Problem (35) is a SDP problem and can be solved by the CVX tool [37]. The procedure for optimizing passive beamforming is sketched in **Algorithm 3**.

Algorithm 3 Proposed passive beamforming optimization algorithm

---

1: Initialize $\mathbf{V}^{(0)}$ and $\rho^{(0)}$. Set $\varepsilon^{(t_3)} = 0$ and $t_3 = 0$.
2: **repeat**
3:     Solve problem (35) with $\left\{\varepsilon^{(t_3)}, \mathbf{V}^{(t_3)}\right\}$ to obtain $\mathbf{V}^*$;
4:     **if** problem (35) is solvable
5:         Update $\mathbf{V}^{(t_3+1)} = \mathbf{V}^*$;
6:         Update $\rho^{(t_3+1)} = \rho^{(0)}$;
7:     **else**
8:         Update $\mathbf{V}^{(t_3+1)} = \mathbf{V}^{(t_3)}$;
9:         update $\rho^{(t_3+1)} = \frac{\rho^{(t_3)}}{2}$;
10:    **end**
11:   Update $\varepsilon^{(t_3+1)}$ via (34);
12:   Update $t_3 = t_3 + 1$;
13: **until** $\frac{\text{Tr}\left(\mathbf{V}^{(t_3)}\right)}{\lambda_{\max}\left(\mathbf{V}^{(t_3)}\right)}$ is below a predefined threshold and the objective value of problem (35) converges.
14: **Output**: $\mathbf{V}$.

C. Proposed Algorithm, Complexity and Convergence

To facilitate the understanding of the proposed IBCD algorithm for solving problem (17), we summarize it in **Algorithm 4**. The convergence of **Algorithm 4** is analyzed as follows. **Algorithm 1** and **Algorithm 3** converge to a KKT stationary solution of problem (18) and problem (32), respectively. Similar proofs can be found in [36] and [34]. Furthermore, the objective value of problem (17) is non-decreasing after each iteration and the radar beampattern gain is upper bounded. Therefore, the proposed IBCD algorithm is guaranteed to converge. Let $T_1^{\max}$ and $T_2^{\max}$ denote the number of iterations of **Algorithm 1** and **Algorithm 2**. Then, the complexity of **Algorithm 1** is given by $\mathcal{O}\left(T_1^{\max}O_1 + T_2^{\max}O_2\right)$, where O_i is defined as

$$O_i = \max\left\{3K + Q + 1, N\right\}^4 \sqrt{N} \log \frac{1}{\varpi_i}, \tag{36}$$

where ϖ_1 and ϖ_2 are the solution accuracies of **Algorithm 1** and **Algorithm 2**, $i \in \{1, 2\}$.

Similarly, the complexity of **Algorithm 3** is given by $\mathcal{O}\left(T_3^{\max} O_3\right)$ with

$$O_3 = \max\left\{3K + Q + 1, M\right\}^4 \sqrt{M} \log \frac{1}{\varpi_3}, \tag{37}$$

where $T_3^{\max}$ and ϖ_3 are the corresponding number of iterations and solution accuracy, respectively.

Finally, the total complexity of **Algorithm 4** is given by

$$\mathcal{O}\left(T_4^{\max}\left(T_1^{\max} O_1 + T_2^{\max} O_2 + T_3^{\max} O_3\right)\right), \tag{38}$$

where $T_4^{\max}$ is the number of iterations of **Algorithm 4**.

Algorithm 4 Proposed IBCD algorithm for solving problem (10)

1: Initialize $\mathbf{V}^{(0)}$ and set $t_4 = 0$.
2: **repeat**
3:    $t_4 = t_4 + 1$;
4:    update $\mathbf{W}_k^{(t_4)}$ and $\mathbf{a}_k^{(t_4)}$ by **Algorithm 1** with $\mathbf{V}^{(t_4-1)}$;
5:    update $\mathbf{V}^{(t_4)}$ by **Algorithm 3** with $\mathbf{W}_k^{(t_4)}$ and $\mathbf{a}_k^{(t_4)}$;
6: **until** the objective value of problem (17) converges.
7: **Output**: $\mathbf{W}_k$, $\mathbf{a}_k$, and $\mathbf{V}$, $k \in \mathcal{K}$.

IV. LOW COMPLEXITY ALGORITHM

In the developed **Algorithm 4**, $\{\mathbf{W}_k\}$ and $\{\mathbf{a}_k\}$ are jointly optimized by applying **Algorithm 1**. However, the computational complexity of **Algorithm 1** scales linearly with $T_1^{\max}$ and $T_2^{\max}$. Note that the joint optimization strategy over $\{\mathbf{W}_k\}$ and $\{\mathbf{a}_k\}$ can achieve better performance than other benchmark schemes, which will be revealed via simulations in Section V. To strike a balance between the performance and computational complexity, we develop a low-complexity algorithm based on the IAO method, where the active beamforming, power allocation coefficients and passive beamforming are optimized iteratively in an alternating manner. In each iteration, the passive beamforming solution is also obtained by **Algorithm 3**. However, the active beamforming is optimized by a single SDP problem and the solutions of the power allocation coefficients are obtained by a proposed closed-form power allocation strategy. To begin with, we first exploit the feasibility of problem (17).

Theorem 2. *Given the active beamforming matrix $\{\mathbf{W}_k\}$ and passive beamforming matrix $\mathbf{V}$, problem* (17) *is feasible, if and only if the following inequality holds:*

$$\max\left(a_{k,f}^{\min,1}, a_{k,f}^{\min,2}\right) \leqslant a_{k,f}^{\max} < 1, \tag{39}$$

where $a_{k,f}^{\max}$, $a_{k,f}^{\min,1}$ and $a_{k,f}^{\min,2}$ are, respectively, defined as

$$a_{k,f}^{\max} = 1 - \frac{r_{k,n}^{\min}\left[\sum_{\tilde{k}\neq k}^{K} \mathrm{Tr}\left(\mathbf{W}_{\tilde{k}}\mathbf{H}_{k,n}\right) + \sigma^2\right]}{\mathrm{Tr}\left(\mathbf{W}_k\mathbf{H}_{k,n}\right)}, \tag{40}$$

$$a_{k,f}^{\min,1} = \frac{\mathrm{Tr}\left(\mathbf{W}_k\mathbf{H}_{k,n}\right) + \sum_{\tilde{k}\neq k}^{K}\left(\mathbf{W}_{\tilde{k}}\mathbf{H}_{k,n}\right) + \sigma^2}{\left(1 + \frac{1}{r_{k,f}^{\min}}\right)\mathrm{Tr}\left(\mathbf{W}_k\mathbf{H}_{k,n}\right)}, \tag{41}$$

$$a_{k,f}^{\min,2} = \frac{\mathrm{Tr}\left(\mathbf{W}_k\mathbf{H}_{k,f}\right) + \sum_{\tilde{k}\neq k}^{K}\mathrm{Tr}\left(\mathbf{W}_{\tilde{k}}\mathbf{H}_{k,f}\right) + \sigma^2}{\left(1 + \frac{1}{r_{k,f}^{\min}}\right)\mathrm{Tr}\left(\mathbf{W}_k\mathbf{H}_{k,f}\right)}. \tag{42}$$

Proof: Please refer to Appendix B.

Following the idea introduced in [38], in each cluster, the power allocation should be first performed for the RFU and only necessary power should be allocated to satisfy the minimum QoS constraints. Then, the remaining power should be allocated to the RNU. According to the minimum QoS constraints (14) and (15), if $a_{k,f}$ is a feasible solution of problem (17), we have: $a_{k,f} \geqslant \max\left\{a_{k,f}^{\min,1}, a_{k,f}^{\min,2}\right\}$. Finally, the closed-form power allocation coefficients are given by:

$$a_{k,f} = \max\left\{a_{k,f}^{\min,1}, a_{k,f}^{\min,2}\right\} \text{ and } a_{k,n} = 1 - \max\left\{a_{k,f}^{\min,1}, a_{k,f}^{\min,2}\right\}, k \in \mathcal{K}. \tag{43}$$

For any given $\{\mathbf{a}_k\}$ and $\mathbf{V}$, the optimization problem for the design of $\{\mathbf{W}_k\}$ is expressed as follows

$$\max_{\chi > 0, \mathbf{W}_k \succcurlyeq 0} \chi, \tag{44a}$$

$$\text{s.t. (13), (14), (15), (16b), (16d), (17b).} \tag{44b}$$

Similar to tackling the rank-one constraint in problem (18), we solve problem (44) by employing SDR and removing the rank-one in constraint (16d). The tightness of the SDR method for problem (44) can be proved by the following theorem.

Theorem 3. *The optimal solution $\mathbf{W}_k$ satisfying $\mathrm{rank}\left(\mathbf{W}_k\right) \leqslant 1$ can always be obtained by solving problem* (44) *without rank-one constraint.*

*Proof: The proof follows similar arguments as that of **Theorem 1** and is thus omitted for brevity.*

The overall proposed IAO algorithm is summarized in **Algorithm 5**. Similar to **Algorithm 4**, the objective value obtained in **Algorithm 5** is non-decreasing in each iteration and the proposed

algorithm is guaranteed to converge. **Algorithm 5** is computationally efficient as $\{\mathbf{W}_k\}$ in step 4 are updated by solving the SDP problem (44) and $\{\mathbf{a}_k\}$ in step 6 are updated by using closed-form expressions without iterations. The computational complexity of problem (44) in solving the SDP problem can be represented by $\mathcal{O}\left(\max\{3K+Q+1, N\}^4 \sqrt{N} \log \frac{1}{\varpi_5}\right)$, where ϖ_5 is the corresponding solution accuracy. Thus, the overall complexity of **Algorithm 5** can be written as $\mathcal{O}\left(T_5^{\max}\left(\max\{3K+Q+1, N\}^4 \sqrt{N} \log \frac{1}{\varpi_5} + O_3\right)\right)$, where $T_5^{\max}$ is the number of iterations of **Algorithm 5**.

Algorithm 5 Proposed IAO algorithm for solving problem (10)

1: Initialize $\left\{\mathbf{a}_k^{(0)}\right\}$ and $\mathbf{V}^{(0)}$ and set the iteration index $t_5 = 0$.
2: **repeat**
3:   $t_5 = t_5 + 1$;
4:   For a given $\mathbf{a}_k^{(t_5-1)}$ and $\mathbf{V}^{(t_5-1)}$, update $\mathbf{W}_k^{(t_5)}$ by solving problem (44) without constraint (16d) ;
5:   For a given $\mathbf{W}_k^{(t_5)}$ and $\mathbf{a}_k^{(t_5-1)}$, update $\mathbf{V}^{(t_5)}$ by applying **Algorithm 3**;
6:   For a given $\mathbf{W}_k^{(t_5)}$ and $\mathbf{V}^{(t_2)}$, update $\mathbf{a}_k^{(t_5)}$ according to (43);
7: **until** the objective value of problem (17) converges.
8: **Output**: $\mathbf{W}_k$, $\mathbf{a}_k$, and $\mathbf{V}$, $k \in \mathcal{K}$.

V. SIMULATION RESULTS

In this section, the performance of the proposed algorithms for the RIS-NOMA-ISAC system is evaluated through numerical simulations. The simulated RIS-NOMA-ISAC system geometry is shown in Fig. 2. We assume that there are three clusters and three radar targets. The RIS is located at the origin, while the BS is located at $(-40, 10)$ meter (m). In each cluster, the RNU and the RFU are randomly distributed on the half circles centered at $(0, 0)$ m with radii of $r_{k,n} \in [20, 25]$ m and $r_{k,f} \in [80, 85]$ m, respectively. Let $\theta_{k,i}$ denote the angle from the RIS to user $\mathrm{U}(k, i)$ and we further assume that $\{\theta_{1,i}\}$, $\{\theta_{2,i}\}$, and $\{\theta_{3,i}\}$, which denote the set of angles of Cluster 1, 2 and 3, are randomly distributed in the angle ranges $(-30^\circ, -20^\circ]$, $(20^\circ, 30^\circ]$, and $(60^\circ, 70^\circ]$, respectively. Without loss of generality, let $\theta_{k,n} = \theta_{k,f}$, $k \in \mathcal{K}$. The angles from the RIS to the three targets are set to be -45°, 0° and 45°, and the corresponding radii are set to be 90 m, 90 m and 80 m, respectively. Given the angles of sensing targets, the desired beampattern can be defined as

$$\mathcal{P}(\theta) = \begin{cases} 1, \theta_{\mathrm{T}} - \frac{\Delta\theta}{2} \leqslant \theta \leqslant \theta_{\mathrm{T}} + \frac{\Delta\theta}{2}, \theta_{\mathrm{T}} \in \{-45^\circ, 0^\circ, 45^\circ\}, \\ 0, \text{otherwise}, \end{cases} \tag{45}$$
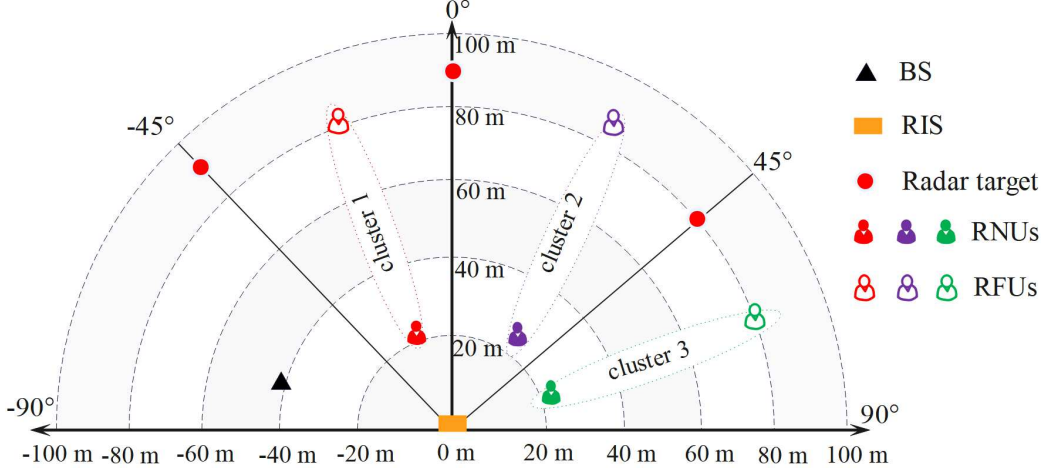
Fig. 2: The simulated RIS-NOMA-ISAC system geometry.

where $\Delta\theta = 6^\circ$ is the desired beam width, θ is the element of the angle grid $\left[-90^\circ : \frac{180^\circ}{100} : 90^\circ\right]$, and the interested sensing angle set can be defined as $\mathcal{Q}_\theta = \left\{ \theta \left| \begin{array}{l} \theta_{\mathrm{T}} - \frac{\Delta\theta}{2} \leqslant \theta \leqslant \theta_{\mathrm{T}} + \frac{\Delta\theta}{2}, \\ \theta_{\mathrm{T}} \in \{-45^\circ, 0^\circ, 45^\circ\} \end{array} \right. \right\}$.

We further assume that all the channels follow the Rician fading distribution, which can be modeled as follows [39, 40]:

$$\mathbf{G} = \sqrt{\varepsilon_0 d_{\mathrm{BR}}^{-\varpi_{\mathrm{BR}}}} \left(\sqrt{\frac{\kappa_{\mathrm{BR}}}{1 + \kappa_{\mathrm{BR}}}} \mathbf{G}_{\mathrm{LoS}} + \sqrt{\frac{1}{1 + \kappa_{\mathrm{BR}}}} \mathbf{G}_{\mathrm{NLoS}} \right), \tag{46}$$

$$\mathbf{g}_{k,i} = \sqrt{\varepsilon_0 d_{\mathrm{R},(k,i)}^{-\varpi_{\mathrm{R},(k,i)}}} \left(\sqrt{\frac{\kappa_{\mathrm{R},(k,i)}}{1 + \kappa_{\mathrm{R},(k,i)}}} \mathbf{g}_{\mathrm{R},(k,i)}^{\mathrm{LoS}} + \sqrt{\frac{1}{1 + \kappa_{\mathrm{R},(k,i)}}} \mathbf{g}_{\mathrm{R},(k,i)}^{\mathrm{NLoS}} \right), \tag{47}$$

where ε_0 denotes the path loss at a reference distance of one meter, ϖ_{BR} and $\varpi_{\mathrm{R},(k,i)}$ denote the path loss exponents, κ_{BR} and $\kappa_{\mathrm{R},(k,i)}$ denote the Rician factors, $\mathbf{G}_{\mathrm{LoS}}$ and $\mathbf{g}_{\mathrm{R},(k,i)}^{\mathrm{LoS}}$ are the LoS components of channel $\mathbf{G}$ and $\mathbf{g}_{k,i}$, $\mathbf{G}_{\mathrm{NLoS}}$ and $\mathbf{g}_{\mathrm{R},(k,i)}^{\mathrm{NLoS}}$ are the corresponding NLoS components. The LoS component is modeled as the product of the array response vectors of the transceivers and the NLoS component is modeled as Rayleigh fading. Without loss of generality, we assume that the path loss exponents and the Rician factors for all channels are identical. The path loss at a reference distance of one meter is set to 30 dB, the path loss exponents are set to 2.2, the Rician factors are set to 3, the noise power is set to -90 dBm, the normalized spacing between two adjacent antennas(elements) is set as $\frac{d}{\lambda} = 0.5$. Other system parameters are set as follows unless specified otherwise later: the maximum transmit power is set to 35 dBm, the minimum QoS requirement for RNUs and RFUs are set to $R_{k,n}^{\min} = 0.5$ bits/s/Hz and $R_{k,f}^{\min} = 0.1$ bits/s/Hz, respectively. Unless otherwise stated, we adopt the default values of the system parameters

TABLE I: Simulation Parameters

Parameter	Value
Locations of the BS and RIS	$(-40, 10)\,\mathrm{m}$ and $(0, 0)\,\mathrm{m}$
Angles of the three radar targets	$-45º$, $0º$, and $45º$
Radius from the RIS to the three radar targets	90m, 90m, and 80m
Angle ranges of the three clusters	$(-30º, -20º]$, $(20º, 30º]$, and $(60º, 70º]$
Radius ranges from the RIS to RNUs and RFUs	$[20, 25]\,\mathrm{m}$ and $[80, 85]\,\mathrm{m}$
Minimum QoS requirement for RNUs and RFUs	0.5 bits/s/Hz and 0.1 bits/s/Hz
Maximum transmit power	35 dBm
Path loss exponents and Rician factors of all channels	2.2 and 3
Path loss at one meter	30 dB
Desired beam width	$6º$
Noise power	-90 dBm

provided in Table I. All of the following numerical results are obtained by averaging over 100 random channel realizations unless otherwise specified.

A. Convergence and Solutions' Rank of the Proposed Algorithms

1) Convergence: In Fig. 3, we investigate the convergence behavior of the proposed algorithms with different numbers of RIS reflecting elements M and BS antennas N. We observe that, for both cases, the proposed algorithms monotonically converge to stationary points within approximately 10 iterations. Furthermore, the minimum beampattern gain achieved by the IAO algorithm is lower than that of the IBCD algorithm. This behavior will be explained in the following numerical results. Though some performance loss is incurred by the IAO algorithm, the complexity of the IAO algorithm is much lower than that of the IBCD algorithm.

2) Solutions' Rank: Based on **Theorem 1** and **Theorem 3**, the rank-one solutions for active beamforming matrices can always be obtained by the proposed IBCD and IAO algorithms. To verify the Theorems, in Table II, we list the average ratios between the largest eigenvalue and the second largest eigenvalue of the matrices $\{\mathbf{W}_1, \mathbf{W}_2, \mathbf{W}_3\}$ obtained by the proposed algorithms. It is easy to observe that the values of the ratios are always enormous for different values of N and M. On the other hand, we also list this ratio for the passive beamforming matrix $\mathbf{V}$ obtained by **Algorithm 3** in Table II. Obviously, the average ratios achieved by the proposed IBCD and IAO algorithms are sufficiently large. These results in Table II reveal that the solutions obtained by the proposed algorithms always satisfy the rank-one constraints.

TABLE II: The ratios obtained by the proposed algorithms with different N and M.

	M	32		36	
	N	3	12	3	12
IBCD algorithm	$\mathbf{W}_1$	2.4441e+09	6.0565e+09	2.0657e+09	3.7819e+09
	$\mathbf{W}_2$	2.5464e+09	5.4004e+09	2.0341e+09	4.1430e+09
	$\mathbf{W}_3$	2.6132e+09	5.9513e+09	2.1736e+09	4.0795e+09
	$\mathbf{V}$	2.4804e+10	3.0715e+10	2.5339e+10	0.5839e+10
	M	32		36	
	N	3	12	3	12
IAO algorithm	$\mathbf{W}_1$	0.0728e+11	1.7223e+11	2.0472e+10	7.6990e+10
	$\mathbf{W}_2$	0.1226e+11	1.0293e+11	1.0012e+10	5.9330e+10
	$\mathbf{W}_3$	0.1436e+11	1.1674e+11	1.3838e+10	8.1600e+10
	$\mathbf{V}$	1.2814e+11	1.8597e+11	5.9715e+11	3.7944e+11
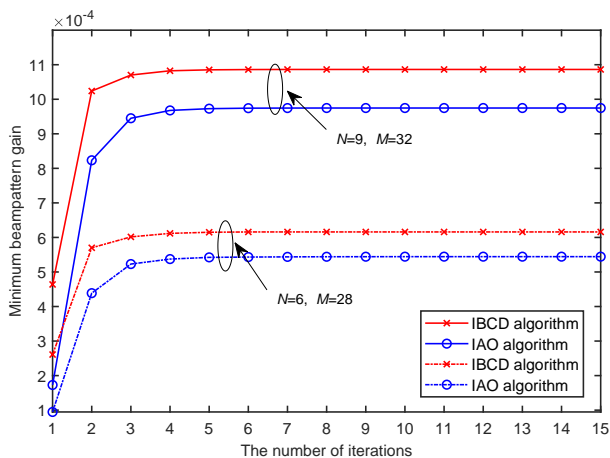
Fig. 3: Convergence of the proposed IBCD algorithm and IAO algorithm.
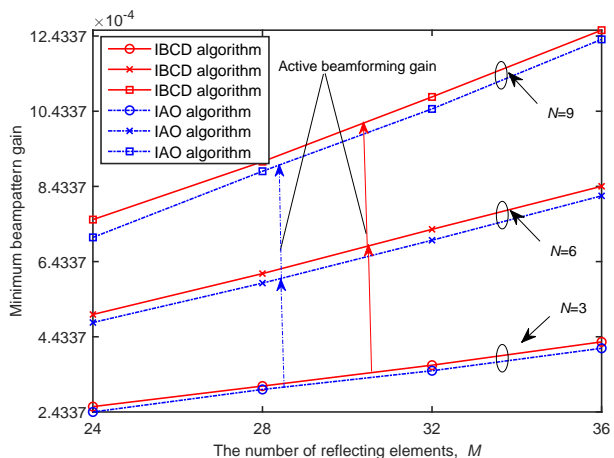
Fig. 4: Minimum beampattern gain versus number of reflecting elements for different N.

B. Performance Analysis of the Proposed Algorithms

Fig. 4 depicts the minimum beampattern gain versus the number of RIS reflecting elements, M, for different numbers of BS antennas. Firstly, it is observed that the minimum beampattern gains obtained by the proposed algorithms monotonically increase with M. This is expected since installing more reflecting elements at RIS can introduce more virtual LoS links and provide higher passive beamforming gain towards the radar targets. Secondly, the proposed low complexity IAO algorithm can achieve comparable performance to that achieved by the IBCD algorithm. Thirdly, we note that the performance of the two proposed algorithms can be improved by increasing N. In fact, more BS antennas introduce more DoFs to construct a more directional sensing beam and to achieve a higher active beamforming gain, thereby increasing minimum beampattern gain.

On the other hand, in Fig. 5, we plot the beampattern gain versus angles. As illustrated in Fig. 5, both proposed schemes can achieve the dominant peaks of the beampattern gain in the angles of interest, i.e., -45°, 0° and 45°. Moreover, at the target directions, the achievable beampattern gains of the IBCD algorithm are always higher than that of the IAO algorithm.
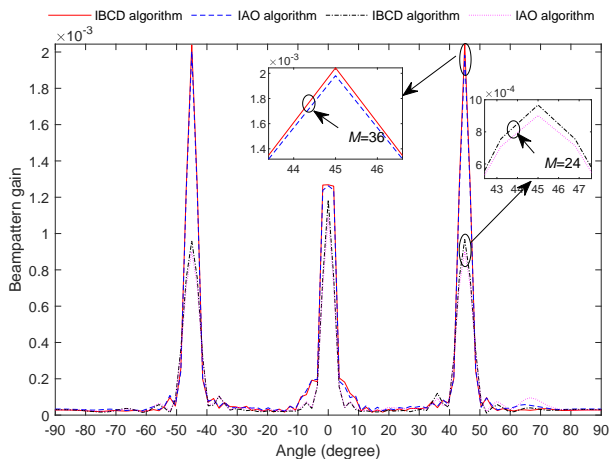
Fig. 5: Beampattern gain versus angles for different M with $N = 9$.
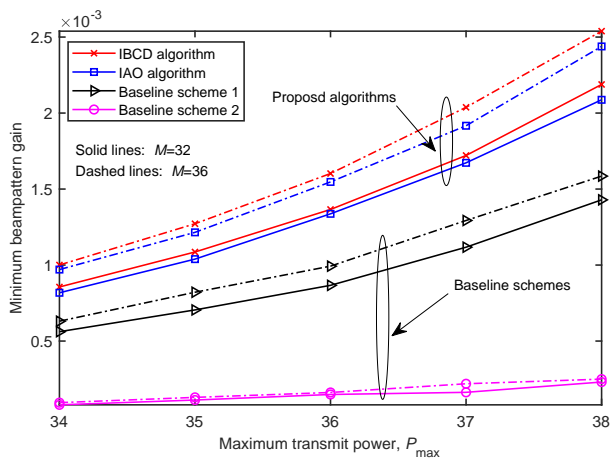
Fig. 6: Minimum beampattern gain versus maximum transmit power, $P_{\max}$, for different schemes with $N = 9$.

C. Comparison With Different Schemes for RIS-NOMA-ISAC System

We compare the performances of the proposed algorithms with two baseline schemes. For baseline scheme 1, the active beamforming design implements an approximate zero-forcing method [41], i.e, only the RNUs in each cluster and the combined channel vector $\mathbf{g}_{k,n}^H \boldsymbol{\Theta} \mathbf{G}$ are utilized to determine each beam. For baseline scheme 2, the active beamforming is realized by the maximum-ratio transmission method [42] based on the RFUs's combined channel gain. We further assume that each cluster shares the same power allocation coefficients in all baseline schemes. For a fair comparison, the resulting optimization problems are solved by applying the SDR or SRCR algorithm [34]. In Fig. 6, we study the minimum beampattern gain versus the maximum transmit power, $P_{\max}$, for all schemes. As expected, the minimum beampattern gain increases as $P_{\max}$ grows. The reason behind this is that when the transmit power is high, the received signal strength at the communication users and targets are strong. The QoS requirements of the communication users can be easily satisfied and more redundant power can be utilized to improve the sensing performance, thereby significantly increasing the beampattern gain. Moreover, it can be seen that the proposed schemes are capable of providing a higher beampattern gain than the baseline schemes. This can be explained by the fact that the active beamforming, power allocation coefficients and passive beamforming are not jointly optimized in the baseline

schemes. However, in the proposed schemes, the joint optimization over these variables can provide a considerable performance improvement and fully exploit the DoFs introduced by the RIS and NOMA.

D. Comparison With Different RIS Assisted Systems

To demonstrate the effectiveness of our proposed RIS-NOMA-ISAC system, we consider the following two benchmark systems:

- RIS-ISAC system: In this system, NOMA is not employed. The achievable rate of user k can be obtained by: $R_k = \log_2\left(1 + \frac{\left|\mathbf{g}_k^H\mathbf{\Theta Gw}_k\right|^2}{\sum_{i\neq k}^{2K}\left|\mathbf{g}_i^H\mathbf{\Theta Gw}_k\right|^2 + \sigma^2}\right)$, where $\mathbf{g}_k$ is the channel coefficients from the RIS to user k, $k \in \{1, 2, \cdots, 2K\}$.

- RIS-Sensing system: In this system, the transmitted signal at the BS is used only for radar sensing while the communication function is not considered during the system design.

Note that the resulting optimization problems for RIS-ISAC system and RIS-Sensing system can be solved in a similar way as solving problem (10). In addition, for the ease of presentation, we focus on the proposed IBCD algorithm for RIS-NOMA-ISAC system.

In Fig. 7, we compare the minimum beampattern gain versus the number of BS antennas, N, for different systems. It is clear that when N increases, which means that more active beams are exploited to transmit the BS signal, higher possible beamforming gain can be provided towards the radar targets. Moreover, the proposed RIS-NOMA-ISAC system outperforms the RIS-ISAC system under overloaded ($N < 6$) and underloaded ($N > 6$) cases. This is because the RIS-NOMA-ISAC system can mitigate the inter-user interference by employing SIC and provide more DoFs for radar sensing. However, the RIS-ISAC system cannot mitigate the inter-user interference effectively. Besides, the RIS-NOMA-ISAC system and the RIS-ISAC system achieve lower performance than the RIS-Sensing system, which reveals a trade-off between the radar sensing and communication for ISAC systems.

On the other hand, we evaluate the normalized beampattern gain of the considered systems with respect to different angles in Fig. 8. As can be observed, the beampattern gains of all systems have peaks towards target directions and our proposed RIS-NOMA-ISAC system has a stronger peak compared with the RIS-ISAC system. Moreover, the proposed RIS-NOMA-ISAC system can obtain higher beampattern gains at the worst angles than the RIS-ISAC system.
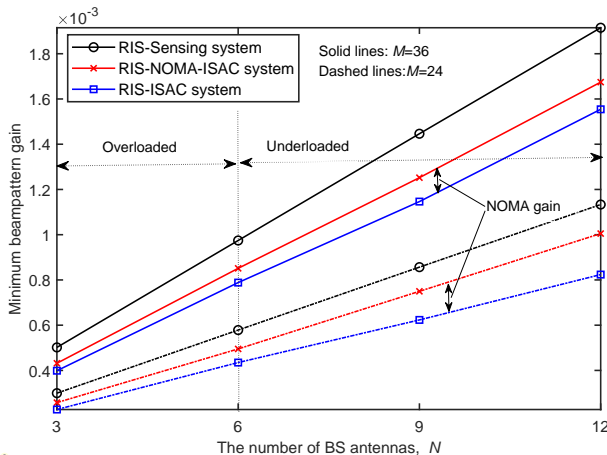
Fig. 7: Minimum beampattern gain versus number of BS antennas for different systems.
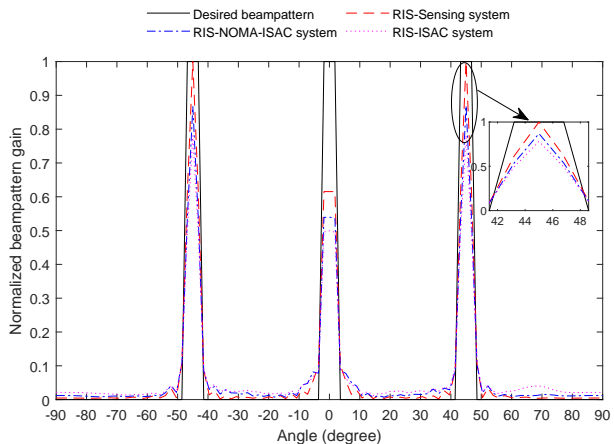
Fig. 8: Normalized beampattern gain versus angles for different systems with $N = 9$ and $M = 36$.

E. Illumination Power

In the previous subsections, the performance of the proposed schemes and system are evaluated by the beampattern gain metric. In this subsection, we adopt an alternative metric, namely, illumination power [22], to evaluate the radar sensing performance. Let $\mathbf{g}_X$ denote the channel from the RIS to any location in the considered system geometry. Then, the illumination power can be defined as $\mathrm{Tr}\left[\mathbf{V}\boldsymbol{\Upsilon}\left(\sum_{k=1}^{K}\mathbf{W}_k\right)\boldsymbol{\Upsilon}^H\right]$, where $\boldsymbol{\Upsilon} = \mathrm{diag}\left\{\mathbf{g}_X^H\right\}\mathbf{G}$. $\mathbf{g}_X$ is modeled as a LoS channel as in [22]. In Fig. 9, we show the illumination power map of the RIS on different angles and locations over one random channel realization. From Fig. 9, we can see that there are three brightest regions towards the three target directions in different systems. This is intuitive since the RIS attempts to steer both the active and passive beamforming towards the targets to maximize the minimum beampattern. Compared with Fig.9(a) for RIS-Sensing system, the leakages of illumination power towards angles of no interest are more serious in Fig. 9(b) for the RIS-NOMA-ISAC system and Fig. 9(c) for the RIS-ISAC system. To further reveal the insights of the illumination power map, in Fig. 10, we present the total illumination power towards the angles of interest for each target, where the angles of interest for the three targets are $[-45^\circ - \Delta\theta, -45^\circ + \Delta\theta]$, $[0^\circ - \Delta\theta, 0^\circ + \Delta\theta]$ and $[45^\circ - \Delta\theta, 45^\circ + \Delta\theta]$, respectively. It is clear that the RIS-Sensing system achieves the best performance. Furthermore, the proposed RIS-NOMA-ISAC system achieves higher illumination power towards the three targets than that of the RIS-ISAC system. These results clearly demonstrate the importance of employing NOMA in the ISAC system.

(a) RIS-Sensing system   (b) RIS-NOMA-ISAC system   (c) RIS-ISAC system
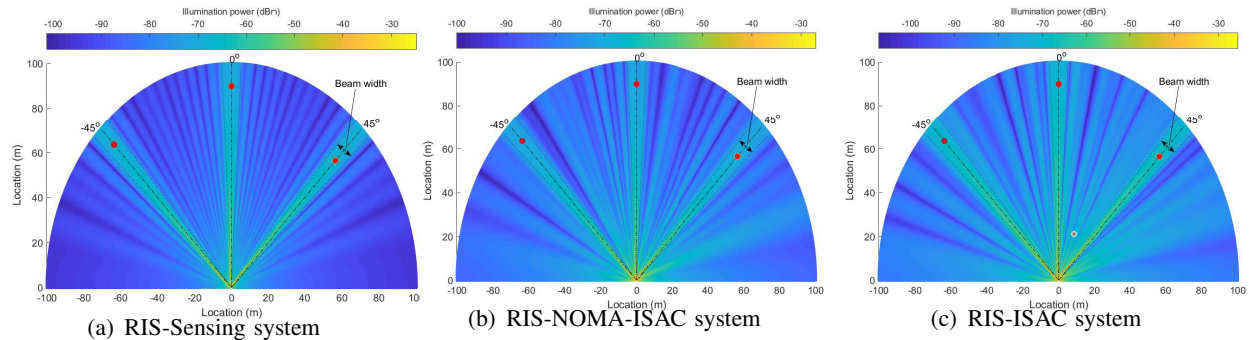
Fig. 9: The map of illumination power for different systems with $N = 12$ and $M = 36$.
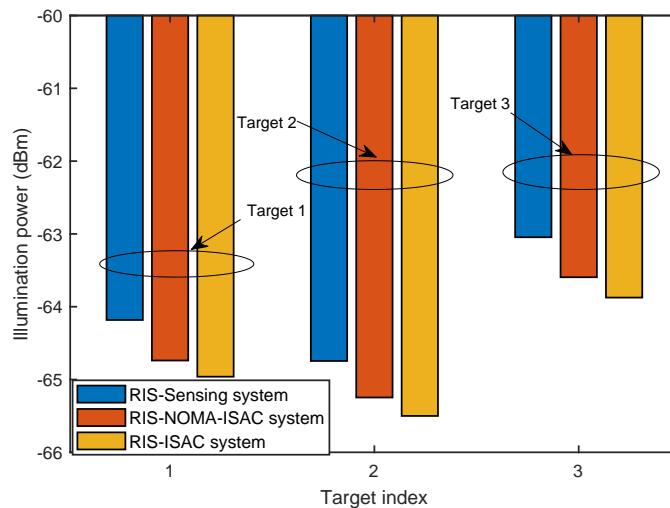
Fig. 10: Illumination power on targets for different systems with $N = 12$ and $M = 36$.

VI. CONCLUSIONS

We proposed a novel RIS-NOMA-ISAC system, where the RIS is deployed to serve the communication users and to assist radar sensing. A joint optimization problem over active beamforming, power allocation coefficients, and passive beamforming was formulated with the aim of maximizing the minimum beampattern gain. Due to the nonconvex nature of the formulated problem, an IBCD algorithm was proposed to solve the original problem. To further reduce the complexity of the proposed algorithm, a low complexity IAO algorithm was proposed where the exact power allocation coefficients are derived in closed-form expressions. Numerical results confirmed that our proposed algorithms can achieve better beampattern gain performance in comparison to other baseline schemes. Moreover, our results revealed that NOMA is an efficient means to mitigate the inter-user interference in ISAC systems whether the system is overloaded or underloaded.

APPENDIX A: PROOF OF THEOREM 1

Since problem (30) is convex and satisfies the Slater's condition, and strong duality holds. The Lagrangian function of problem (30) in terms of beamforming matrices $\{\mathbf{W}_k\}$ is given as follows:

$$
\begin{aligned}
\psi_{\text{Lag}} = & -\alpha_0 \sum_{k=1}^{K} \text{Tr}\left(\mathbf{W}_k\right) - \sum_{k=1}^{K} \beta_k^{\eta} r_{k,n}^{\min} I_{k,n}^{\text{iter}} + \sum_{k=1}^{K} \text{Tr}\left(\mathbf{W}_k \mathbf{X}_k\right) + \varrho \\
& + \sum_{q=1}^{Q} \alpha_q \text{Tr}\left[\left(\sum_{k=1}^{K} \mathbf{W}_k\right) \mathbf{\Upsilon}_q^H \mathbf{V} \mathbf{\Upsilon}_q\right] + \sum_{k=1}^{K} \text{Tr}\left(\mathbf{Y}_k \begin{bmatrix} a_{k,n} & \eta_k \\ \eta_k & \text{Tr}\left(\mathbf{W}_k \mathbf{H}_{k,n}\right) \end{bmatrix}\right) \\
& + \sum_{k=1}^{K} \frac{\beta_k^{\mathcal{T}_1}\left(\text{Tr}\left(\mathbf{W}_k \mathbf{\Gamma}_{k,n}^H \mathbf{V} \mathbf{\Gamma}_{k,n}\right) - r_{k,f}^{\min} I_{k,n}^{\text{iter}}\right)}{\left(1 + r_{k,f}^{\min}\right)} + \sum_{k=1}^{K} \frac{\beta_k^{\mathcal{T}_2}\left(\text{Tr}\left(\mathbf{W}_k \mathbf{\Gamma}_{k,f}^H \mathbf{V} \mathbf{\Gamma}_{k,f}\right) - r_{k,f}^{\min} I_{k,f}^{\text{iter}}\right)}{\left(1 + r_{k,f}^{\min}\right)},
\end{aligned}
\tag{A.1}
$$

where ϱ is the collection of terms that are not relevant for the proof, α_0, β_k^{η}, α_q, $\beta_k^{\mathcal{T}_1}$ and $\beta_k^{\mathcal{T}_2}$ are the Lagrange multipliers. The matrix $\mathbf{Y}_k$ and $\mathbf{X}_k$ are the Lagrange multiplier matrix for the positive semi-definite constraints. Note that there exists at least one $\alpha_0 > 0$, since constraint (16b) is active for the optimal $\mathbf{W}_k$[2].

The Karush-Kuhn-Tucker (KKT) conditions of problem (30) that are relevant to the proof are given as follows:

$$
\text{K1}: \alpha_0, \alpha_q, \beta_k^{\eta}, \beta_k^{\mathcal{T}_1}, \beta_k^{\mathcal{T}_2} \geqslant 0, \mathbf{Y}_k, \mathbf{Z}_k \succeq \mathbf{0}, \quad \text{K2}: \mathbf{W}_k \mathbf{X}_k = \mathbf{0}, \quad \text{K3}: \nabla_{\mathbf{W}_k} \psi_{\text{Lag}} = \mathbf{0}. \tag{A.2}
$$

To proceed, we derive the gradient of ψ_{Lag} explicitly and rewrite K3 as

$$
\mathbf{Z}_k = \alpha_0 \mathbf{I} - \mathbf{\Pi}_k, \tag{A.3}
$$

where the matrix $\mathbf{\Pi}_k$ is defined as

$$
\begin{aligned}
\mathbf{\Pi}_k = & \left[\gamma_k \left(r_{k,f}^{\min} a_{k,n} - a_{k,f}\right) + \eta_k \left(r_{k,f}^{\min} a_{k,n} - a_{k,f}\right) - \beta_k a_{k,n}\right] \mathbf{H}_{k,n}^H \\
& + \sum_{\widetilde{k} \neq k}^{K} \left(\beta_{\widetilde{k}} r_{\widetilde{k},n}^{\min} + \gamma_{\widetilde{k}} r_{\widetilde{k},f}^{\min} + \eta_{\widetilde{k}} r_{\widetilde{k},f}^{\min}\right) \mathbf{H}_{\widetilde{k},n}^H - \sum_{q=1}^{Q} \mu_q \mathbf{H}_q^H.
\end{aligned}
\tag{A.4}
$$

Denote by $\lambda_{\max}\left(\mathbf{\Pi}_k\right)$ the largest eigenvalue of matrix $\mathbf{\Pi}_k$. Due to the randomness of the channels, the largest eigenvalue $\lambda_{\max}\left(\mathbf{\Pi}_k\right)$ is unique. Recalling the expression (A.3), if $\lambda_{\max}\left(\mathbf{\Pi}_k\right) >$

---

[2]It is easy to prove that constraint (16b) is active by the contradiction method. Specifically, if the equality in constraint (16b) is not satisfied, i.e, $\sum_{k=1}^{K} \text{Tr}\left(\mathbf{W}_k\right) < P_{\max}$. Define $\rho = \frac{P_{\max}}{\sum_{k=1}^{K} \text{Tr}\left(\mathbf{W}_k\right)} > 1$ and multiply ρ by the optimal $\mathbf{W}_k$. As a result, a new solution $\overline{\mathbf{W}}_k$ is obtained. Since the beampattern gain with $\overline{\mathbf{W}}_k$ is larger than that with $\mathbf{W}_k$, which contradicts with the optimality of $\mathbf{W}_k$. Thus, the equality in constraint (16b) always holds.

α_0, then we have: $\alpha_0 \mathbf{I} - \mathbf{\Pi}_k \prec \mathbf{0}$ which contradicts with $\mathbf{Z}_k \succeq \mathbf{0}$. In addition, if $\lambda_{\max} (\mathbf{\Pi}_k) \leqslant \alpha_0$, we have: $\alpha_0 \mathbf{I} - \mathbf{\Pi}_k \succeq \mathbf{0}$, which implies that $\mathbf{Z}_k \leqslant \mathbf{0}$ and $\mathrm{rank} (\mathbf{Z}_k) \geqslant N_{\mathrm{T}} - 1$. Considering K2, we have: $\mathrm{rank} (\mathbf{W}_k) \leqslant 1$. The proof is completed.

APPENDIX B: PROOF OF THEOREM 2

According to the QoS constraint (13) and (10d), we have the following inequalities:

$$a_{k,f} \leqslant 1 - \frac{r_{k,n}^{\min} \left[\sum_{\widetilde{k} \neq k}^{K} \mathrm{Tr} \left(\mathbf{W}_{\widetilde{k}} \mathbf{H}_{k,n} \right) + \sigma^2 \right]}{\mathrm{Tr} \left(\mathbf{W}_k \mathbf{H}_{k,n} \right)} \triangleq a_{k,f}^{\max}. \tag{B.1}$$

In addition, the QoS constraints (14) and (15) can be respectively rewritten as:

$$a_{k,f} \geqslant \frac{\mathrm{Tr} \left(\mathbf{W}_k \mathbf{H}_{k,n} \right) + \sum_{\widetilde{k} \neq k}^{K} \left(\mathbf{W}_{\widetilde{k}} \mathbf{H}_{k,n} \right) + \sigma^2}{\left(1 + \frac{1}{r_{k,f}^{\min}} \right) \mathrm{Tr} \left(\mathbf{W}_k \mathbf{H}_{k,n} \right)} \triangleq a_{k,f}^{\min,1}, \tag{B.2}$$

$$a_{k,f} \geqslant \frac{\mathrm{Tr} \left(\mathbf{W}_k \mathbf{H}_{k,f} \right) + \sum_{\widetilde{k} \neq k}^{K} \mathrm{Tr} \left(\mathbf{W}_{\widetilde{k}} \mathbf{H}_{k,f} \right) + \sigma^2}{\left(1 + \frac{1}{r_{k,f}^{\min}} \right) \mathrm{Tr} \left(\mathbf{W}_k \mathbf{H}_{k,f} \right)} \triangleq a_{k,f}^{\min,2}. \tag{B.3}$$

Combing (B.1), (B.2) and (B.3), it is easy to observe that if problem (17) is feasible, the following condition should be satisfied:

$$\max \left(a_{k,f}^{\min,1}, a_{k,f}^{\min,2} \right) \leqslant a_{k,f}^{\max} < 1. \tag{B.4}$$

REFERENCES

[1] J. Zuo and Y. Liu, "Reconfigurable intelligent surface assisted NOMA empowered integrated sensing and communication," *IEEE GLOBECOM Workshop on NGMA for Future Wireless Communications*, Rio de Janeiro, Brazil, 4–8 Dec. 2022.

[2] J. A. Zhang, M. L. Rahman, K. Wu, X. Huang, Y. J. Guo, S. Chen, and J. Yuan, "Enabling joint communication and radar sensing in mobile networks—a survey," *IEEE Commun. Surv. Tut.*, vol. 24, no. 1, pp. 306–345, Oct. 2022.

[3] F. Dong, F. Liu, Y. Cui, W. Wang, K. Han, and Z. Wang, "Sensing as a service in 6G perceptive networks: a unified framework for ISAC resource allocation," 2022, [Online]. Available: https://arxiv.org/abs/2202.09969.

[4] Z. Wei, F. Liu, C. Masouros, N. Su, and A. P. Petropulu, "Toward multi-functional 6G wireless networks: integrating sensing, communication, and security," *IEEE Commun. Mag.*, vol. 60, no. 4, pp. 65–71, April 2022.

[5] X. Li, Y. Cui, J. A. Zhang, F. Liu, X. Jing, and O. A. Dobre, "Assisting living by wireless sensing: the role of integrated sensing and communications in 6G era," 2022, [Online]. Available: https://arxiv.org/abs/2202.09522.

[6] R. Liu, M. Li, H. Luo, Q. Liu, and A. L. Swindlehurst, "Integrated sensing and communication with reconfigurable intelligent surfaces: opportunities, applications, and future directions," 2022, [Online]. Available: https://arxiv.org/abs/2206.08518.

[7] Z. Gao, Z. Wan, D. Zheng, S. Tan, C. Masouros, D. W. K. Ng, and S. Chen, "Integrated sensing and communication with mmwave massive MIMO: a compressed sampling perspective," 2022, [Online]. Available: https://arxiv.org/abs/2201.05766.

[8] C. Qi, W. Ci, J. Zhang, and X. You, "Hybrid beamforming for millimeter wave MIMO integrated sensing and communications," *IEEE Commun. Lett.*, vol. 26, no. 5, pp. 1136–1140, 2022.

[9] B. Liu, J. Liu, and N. Kato, "Optimal beamformer design for millimeter wave dual-functional radar-communication based V2X systems," *IEEE J. Sel. Areas Commun.*, pp. 1–1, 2022.

[10] C. Chaccour, W. Saad, O. Semiari, M. Bennis, and P. Popovski, "Joint sensing and communication for situational awareness in wireless THz systems," 2021, [Online]. Available: https://arxiv.org/abs/2111.14044.

[11] B. Chang, W. Tang, X. Yan, X. Tong, and Z. Chen, "Integrated scheduling of sensing, communication, and control for mmWave/THz communications in cellular connected UAV networks," *IEEE J. Sel. Areas Commun.*, vol. 40, no. 7, pp. 2103–2113, July 2022.

[12] A. M. Elbir, K. V. Mishra, S. Chatzinotas, and M. Bennis, "Terahertz-band integrated sensing and communications: challenges and opportunities," 2022, [Online]. Available: https://arxiv.org/abs/2208.01235.

[13] L. You, X.-H. Qiang, C. G. Tsinos, F. Liu, W. Wang, X. Gao, and B. E. Ottersten, "Beam squint-aware integrated sensing and communications for hybrid massive MIMO LEO satellite systems," 2022, [Online]. Available: https://arxiv.org/abs/2203.00235.

[14] K. Meng, Q. Wu, S. Ma, W. Chen, K. Wang, and J. Li, "Throughput maximization for UAV-enabled integrated periodic sensing and communication," *IEEE Trans. Wireless Commun. (Early Access)*, 2022.

[15] Y. Liu, S. Zhang, X. Mu, Z. Ding, R. Schober, N. Al-Dhahir, E. Hossain, and X. Shen, "Evolution of NOMA toward next generation multiple access (NGMA) for 6G," *IEEE J. Sel. Areas Commun.*, vol. 40, no. 4, pp. 1037–1071, 2022.

[16] J. Zuo, Y. Liu, Z. Qin, and N. Al-Dhahir, "Resource allocation in intelligent reflecting surface assisted NOMA systems," *IEEE Trans. Commun.*, vol. 68, no. 11, pp. 7170–7183, Nov. 2020.

[17] X. Mu, Y. Liu, L. Guo, J. Lin, and L. H. Hanzo, "NOMA-aided joint radar and multicast-unicast communication systems," *IEEE J. Sel. Areas Commun.*, vol. 40, no. 6, pp. 1978–1992, June 2022.

[18] Z. J. Wang, Y. Liu, X. Mu, Z. Ding, and O. A. Dobre, "NOMA empowered integrated sensing and communication," *IEEE Commun. Lett."*, vol. 26, no. 3, pp. 677–681, March 2022.

[19] Z. J. Wang, Y. Liu, X. Mu, and Z. Ding, "NOMA inspired interference cancellation for integrated sensing and communication," 2021, [Online]. Available: https://arxiv.org/abs/2206.00377.

[20] C. Zhang, W. Yi, Y. Liu, and L. H. Hanzo, "Semi-integrated-sensing-and-communication (semi-ISaC): from OMA to NOMA," 2022, [Online]. Available: https://arxiv.org/abs/2204.11245.

[21] Y. Liu, X. Liu, X. Mu, T. Hou, J. Xu, M. Di Renzo, and N. Al-Dhahir, "Reconfigurable intelligent surfaces: principles and opportunities," *IEEE Commun. Surv. Tut*, vol. 23, no. 3, pp. 1546–1577, May 2021.

[22] R. S. P. Sankar, S. P. Chepuri, and Y. C. Eldar, "Beamforming in integrated sensing and communication systems with reconfigurable intelligent surfaces," 2022, [Online]. https://arxiv.org/abs/2206.07679.

[23] M. Hua, Q. Wu, C. He, S. Ma, and W. Chen, "Joint active and passive beamforming design for IRS-aided radar-communication," 2022, [Online]. Available: https://arxiv.org/abs/2203.14532.

[24] Z. Xing, R. Wang, and X. Yuan, "Passive beamforming design for reconfigurable intelligent surface enabled integrated sensing and communication," 2022, [Online]. Available: https://arxiv.org/abs/2206.00525.

[25] Z. Zhu, Z. Li, Z. Chu, G. Sun, W. Hao, P. Xiao, and I. Lee, "Resource allocation for IRS assisted mmwave integrated sensing and communication systems," *IEEE International Conference on Communications*, Seoul, Korea, 16-20 May, 2022.

[26] X. Liu, H. J. Zhang, K. Long, M. Zhou, Y. Li, and H. V. Poor, "Proximal policy optimization-based transmit beamforming and phase-shift design in an IRS-aided ISAC system for the THz band," *IEEE J. Sel. Areas Commun.*, vol. 40, pp. 2056–2069, July 2022.

[27] X. Song, D. Zhao, H. Hua, T. X. Han, X. Yang, and J. Xu, "Joint transmit and reflective beamforming for IRS-assisted integrated sensing and communication," *IEEE Wireless Communications and Networking Conference (WCNC)*, Austin TX USA, 10-13 April, 2022.

[28] X. Song, J. Xu, F. Liu, T. X. Han, and Y. C. Eldar, "Intelligent reflecting surface enabled sensing: Cramer-Rao lower bound optimization," 2022, [Online]. Available: https://arxiv.org/abs/2204.11071.

[29] Z.-J. Wang, X. Mu, and Y. Liu, "STARS enabled integrated sensing and communications," 2022, [Online]. Available: https://arxiv.org/abs/2207.10748.

[30] J. Cui, Z. Ding, P. Fan, and N. Al-Dhahir, "Unsupervised machine learning-based user clustering in millimeter-wave-NOMA systems," *IEEE Trans. Wireless Commun.*, vol. 17, no. 11, pp. 7425–7440, Nov. 2018.

[31] L. Dai, B. Wang, M. Peng, and S. Chen, "Hybrid precoding-based millimeter-wave massive MIMO-NOMA with simultaneous wireless information and power transfer," *IEEE J. Sel. Areas Commun.*, vol. 37, Jan. 2019.

[32] J. Zhu, Y. Huang, J. Wang, K. Navaie, and Z. Ding, "Power efficient IRS-assisted NOMA," *IEEE Trans. Commun.*, vol. 69, no. 2, pp. 900–913, Feb. 2021.

[33] K. Wang, J. Cui, Z. Ding, and P. Fan, "Stackelberg game for user clustering and power allocation in millimeter wave-NOMA systems," *IEEE Trans. Wireless Commun.*, vol. 18, no. 5, pp. 2842–2857, May 2019.

[34] P. Cao, J. S. Thompson, and H. V. Poor, "A sequential constraint relaxation algorithm for rank-one constrained problems," *25th European Signal Processing Conference (EUSIPCO)*, Kos, Greece, 28 Aug. 2017.

[35] X. Xie, F. Fang, and Z. Ding, "Joint optimization of beamforming, phase-shifting and power allocation in a multi-cluster IRS-NOMA network," *IEEE Trans. Veh. Technol.*, vol. 70, no. 8, pp. 7705–7717, Aug. 2021.

[36] X. Sun, N. Yang, S. Yan, Z. Ding, D. W. K. Ng, C. Shen, and Z. Zhong, "Joint beamforming and power allocation in downlink NOMA multiuser MIMO networks," *IEEE Trans. Wireless Commun.*, vol. 17, no. 8, pp. 5367–5381, Aug. 2018.

[37] M. Grant and S. Boyd, "CVX: Matlab software for disciplined convex programming, version 2.1," http://cvxr.com/cvx, Mar. 2014.

[38] L. Zhu, J. Zhang, Z. Xiao, X. Cao, D. O. Wu, and X.-G. Xia, "Joint Tx-Rx beamforming and power allocation for 5G millimeter-wave non-orthogonal multiple access networks," *IEEE Trans. Commun.*, vol. 67, no. 7, pp. 5114–5125, July 2019.

[39] Y. Li, M. Jiang, Q. Zhang, and J. Qin, "Joint beamforming design in multi-cluster MISO NOMA reconfigurable intelligent surface-aided downlink communication networks," *IEEE Trans. Commun.*, vol. 69, no. 1, pp. 664–674, Jan. 2021.

[40] X. Yu, D. Xu, D. W. K. Ng, and R. Schober, "IRS-assisted green communication systems: provable convergence and robust optimization," *IEEE Trans. Commun.*, vol. 69, no. 9, pp. 6313–6329, Sep. 2021.

[41] B. Wang, L. Dai, Z. Wang, N. Ge, and S. Zhou, "Spectrum and energy-efficient beamspace MIMO-NOMA for millimeter-wave communications using lens antenna array," *IEEE J. Sel. Areas Commun.*, vol. 35, pp. 2370–2382, Oct. 2017.

[42] Q. Wu and R. Zhang, "Intelligent reflecting surface enhanced wireless network via joint active and passive beamforming," *IEEE Trans. Wireless Commun.*, vol. 18, pp. 5394–5409, 2019.